EUROPEAN ORGANIZATION FOR NUCLEAR RESEARCH

CERN/ISRC/)78-32
12 December 1978

STATUS REPORT ON EXPERIMENT R-108

CERN[1]-Columbia[2]-Oxford[3]-Rockefeller[4] (CCOR) Collaboration

A.L.S. Angelis[3], H.-J. Besch[1], B.J. Blumenfeld[2,1], L. Camilleri[1], T.J. Chapin[4], R.L. Cool[4], C. del Papa[1], L. Di Lella[1], Z. Dimcovski[4], R.J. Hollebeek[2], L.M. Lederman[2], D. Levinthal[2], J.T. Linnemann[4], N. Phinney[3], S.H. Pordes[1], A.F. Rothenberg[4,1], R.W. Rusack[2], A.M. Segar[3], J. Singh[1], A.M. Smith[1], M.J. Tannenbaum[4], J. Wallace-Hadrill[3], J.M. Yelton[3] and K.K. Young[1]

G E N E V A

1978

I. Summary of Operations - Calendar Year 1978

In calendar year 1978, the ISR was scheduled for ∿ 29½ weeks of running, almost exclusively at 31 GeV. During this period the operation of R-108 was as follows : data taking 16½ weeks; special runs and tests 2½ weeks; refrigerator failure- solenoid off 8 weeks; lower quality data (mainly due to drift chamber broken wires) 2½ weeks. Also, during the July ISR shut-down all 336 lead glass blocks were removed from the ISR, calibrated at the PS, and reinstalled at the ISR.

II. Results 1978

a) e^+e^- Pairs.

The 13½ weeks of good data obtained before the solenoid failure on 19 October 1978, correspond to an integrated luminosity of 7.2×10^{37} cm^{-2}. These data have been fully analyzed for e^+e^- pairs (Fig. 1). A continuum is observed for e^+e^- masses from 6.0 to 14.25 GeV/c^2; and a peak containing 35 events is observed in the T region (8.75 to 10.75 GeV/c^2). Preliminary results (integrated luminosity 3.5×10^{37} cm^{-2}) have also been reported at the Tokyo Conference (Appendix I).

b) High p_T π^0.

An important feature of this experiment is the ability to measure high p_T π^0 production simultaneously with the data taken for e^+e^- pairs. Two separate triggers are used.

The inclusive cross section for high p_T π^0 production has been measured at three $\sqrt{s}$ values, 30.7, 53.1 and 62.4 GeV, using data taken at various times between August 1977 and March 1978. (Fig. 2). At lower p_T, in agreement with previous experiments [1], the invariant cross section can be fit by the simple scaling law

$$E\frac{d^3\sigma}{dp^3} = p_T^{-n} F(2p_T/\sqrt{s}) \qquad (1)$$

with the power $n \cong 8$, as shown by the broken lines in Fig. 2. At higher p_T, the results are well above the extrapolation of this fit and are inconsistent with scaling of the form given by equation (1) even if n is

allowed to depend on $x_T = 2p_T/\sqrt{s}$ (Fig. 3). However, in the range $7.5 < p_T < 14.0$ GeV/c, for the $\sqrt{s}$ values 53.1 and 62.4 GeV, n is consistent with having the constant value $n = 5.1 \pm 0.4$. This is significant in terms of constituent scattering models [2], and QCD [3], since the power n is characteristic of the force law between the constituents. These results have been presented at Tokyo and are being published in Physics Letters B (Appendix II).

c) Associated Particles.

The cylindrical drift chambers inside the superconducting solenoid allow the detection over the full azimuth of the charged particles produced in association with any trigger. For π^0 triggers with transverse momenta $p_{Tt} > 7.0$ GeV/c, the azimuthal distributions of associated charged particles as a function of their transverse momentum p_T are shown in Fig. 4. Strong peaks on top of flat backgrounds are observed around both the trigger azimuth ($\phi = 0$), and the azimuth opposite the trigger ($\phi = \pi$), for all bands of associated particle p_T. This striking effect corresponds to the naive picture of jets. The width of these peaks is proportional to the rms transverse momentum, $\langle|p_{out}|\rangle$, perpendicular to the trigger plane. In constituent scattering models [4], $\langle|p_{out}|\rangle$ is a measure of the rms transverse momentum $\langle k_T \rangle$ of the quarks inside each of the colliding protons. A value of $\langle k_T \rangle = 0.85$ GeV/c has been used [3] in order to explain the p_T imbalance in high mass lepton pair production at Fermilab [4]. The results shown in Fig. 5 suggest an even larger value of $\langle k_T \rangle$ and also a dependence of $\langle k_T \rangle$ on the trigger p_{Tt}.

These results have been presented at the Copenhagen Jet Conference and at Tokyo, (Appendix III).

III. Apparatus Improvements 1978

During the past year, we have built cathode read-out proportional chambers which give pulse-height measurement on 1 cm spaced strips. These strip chambers will cover the faces of both arrays of lead-glass shower counters. They give coordinate measurement of tracks and showers, thus assisting in the study of particle correlations, in eliminating background in high p_T π^0 events, and in discriminating electrons and pions.

A first chamber, of sensitive area 1.86 x 1.54m, is now operational, complete with read-out on 128 strips, in front of one of the lead glass arrays (Fig. 6). The second chamber and the complete read-out will be installed during January. We expect that some debugging of the system will be necessary in March when the ISR starts up, so that the system will be fully operational in April.

IV. Request for Running in 1979

In general we would like to run at the highest value of $\sqrt{s}$ = 62.4 GeV, with the highest luminosity possible, since all the reactions under investigation have cross sections that increase with increasing $\sqrt{s}$. However, in order to study in detail the onset of the new power law in high p_T π^0 production (Figs. 2 and 3) we propose to take data also at the 3 values of $\sqrt{s}$, 30.7, 44 and 53.1 GeV. These data will also allow the study of associated particles for all values of $\sqrt{s}$.

A proper measurement of the $\sqrt{s}$ dependence of high p_T π^0 production can only be made by reducing systematic errors to a minimum. In order to achieve this goal, we have two basic requirements. The first is to collect all of the data over a period of time as short as possible; the second is to run with the solenoid at its usual magnetic field B = 1.4 T and with the low β turned on for all values of $\sqrt{s}$. In fact, during the first machine development run by the ISR at $\sqrt{s}$ = 30.7 GeV with the solenoid and low β turned on, excellent conditions for physics were achieved.

The detailed running request is given in Table 1. The estimates of ISR running time assume average luminosities as given in the Table and a running efficiency of 70%. Using an ISR running time of $\sim$ 100 hours per scheduled week, the special request amounts to 10½ weeks out of 26½ weeks scheduled in the preliminary 1979 plan. We request that the other 16 weeks be run at $\sqrt{s}$ = 62.4 GeV at the highest possible luminosity [5].

Finally we have the intention of recalibrating all of the lead glass counters at the PS during the ISR shut-down at present foreseen during the month of July 1979. It is imperative, therefore, that the amounts of ISR running time listed in Table 1 be scheduled during the first three ISR periods in 1979.

Table 1

$\sqrt{s}$ (GeV)	Integrated luminosity (cm^{-2})	Average luminosity ($cm^{-2}\ s^{-1}$)	ISR running time (hours)
30.7	3×10^{36}	5×10^{30}	240
44	10^{37}	10^{31}	400
53.1	2×10^{37}	2×10^{31}	400

REFERENCES AND FOOTNOTES

1) F.W. Büsser, et al., Nuclear Physics B106 (1976) 1, and references quoted therein.

2) S.M. Berman, et al., Phys. Rev. D4 (1971) 3388.
R. Blankenbecler, et al., Phys. Rev. D12 (1975) 3649.

3) R.P. Feynman, et al., CALT-68-651 (1978).

4) S.W. Herb, et al., Phys. Rev. Letters 39 (1977) 252.
W.R. Innes, et al., Phys. Rev. Letters 39 (1977) 1240.

5) The optimum ratio of $\sqrt{s}$ = 62.4 running to $\sqrt{s}$ = 53 running can be estimated for 2 reactions e^+e^- and π^0. For the e^+e^- no scaling test is contemplated, so all the running should be at the $\sqrt{s}$ value with the highest cross section × luminosity. For π^0 with scaling as $p_T^{-n} F(x_T)$, the ratio of integrated luminosities to give optimum errors on n is $L(53)/L(62) = (53/62)^{n-1}$, which equals ½ for n = 5.1.

Figure captions

Fig. 1 : Invariant mass spectrum of same charge and opposite charge electron pairs.

Fig. 2 : Invariant cross-sections (cm^2c^3/GeV^2) for the reaction $p + p \to \pi^0$ + anything versus p_T. Also shown are the data points from ref. 1 with their best fit using Eq. (1) (dashed lines). The cross-section scale corresponds to the data at $\sqrt{s}$ = 62.4 GeV. For $\sqrt{s}$ = 53.1, the data have been divided by a factor of 10; for $\sqrt{s}$ = 30.6, by a factor of 100.

Fig. 3 : The exponent n of Eq. (1) plotted as a function of x_T using the two lowest and two highest $\sqrt{s}$ values.

Fig. 4 : Charged particle correlations for π^0 trigger with $p_{Tt} > 7.0$ GeV/c.
a) Same side azimuthal correlation of charged particles relative to the triggering neutral.
b) Away-side azimuthal correlation of charged particles relative to the triggering neutral.
Five plots corresponding to 1 GeV/c intervals in p_T of the charged particle are shown. The pseudorapidity of the charged particles is restricted to $|\eta| < 0.7$.

Fig. 5 : a) and b) $<|p_{out}|>$ of away-side charged particles relative to the trigger for three sets of trigger p_{Tt}.

Fig. 6 : Five individual events recorded by the strip chamber installed in I-1. The distributions represent the pulse height in 128 strips of 1 cm. The first 64 channels are vertical strips, and the second 64 channels are horizontal strips. The black lines labelled "1092" and "B18" show the location of the triggering lead glass block in each projection.

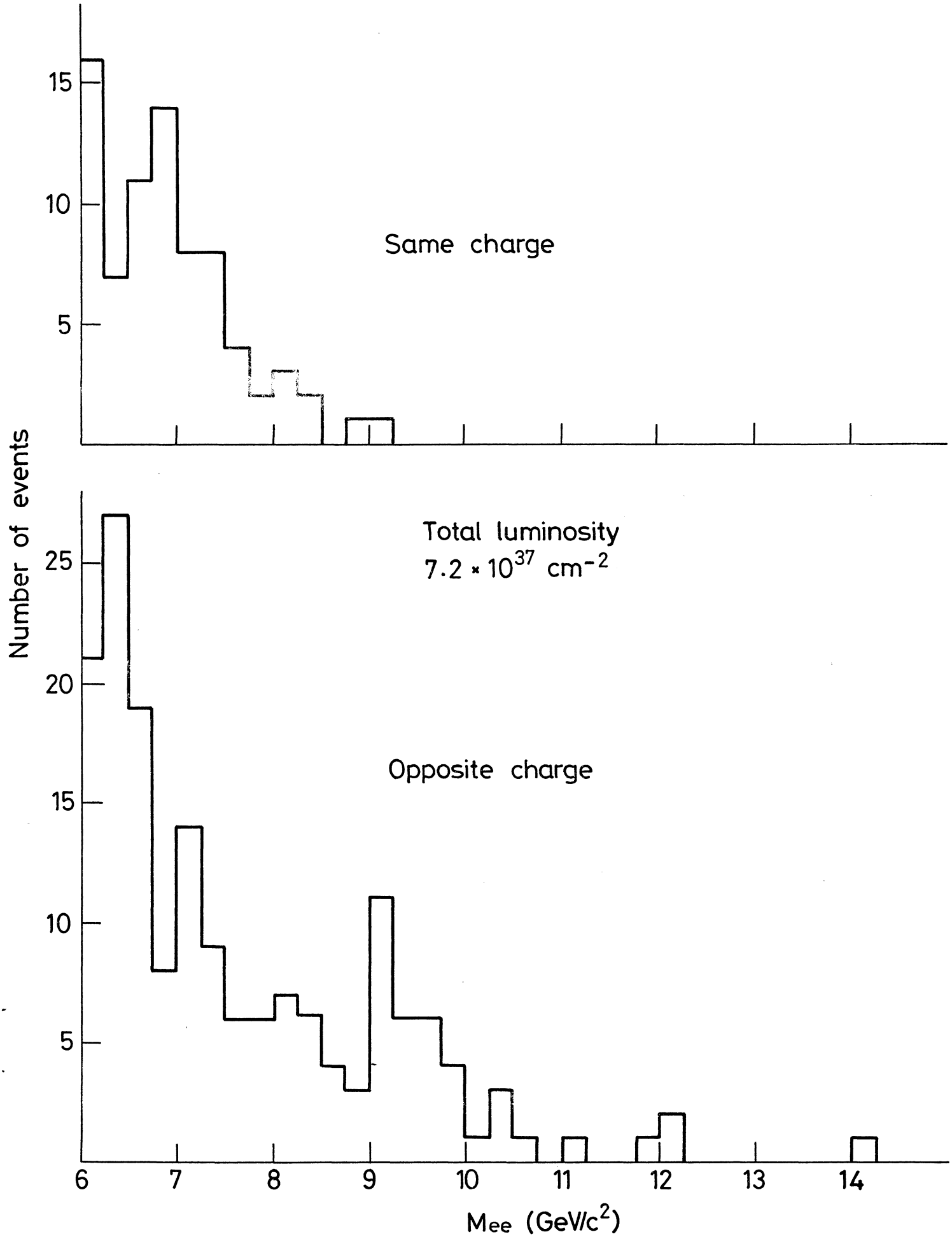
Same charge
Total luminosity
7.2 × 10^37 cm^-2
Opposite charge
Number of events
Mee (GeV/c^2)
15
10
5
25
20
15
10
5
6
7
8
9
10
11
12
13
14

Fig. 1

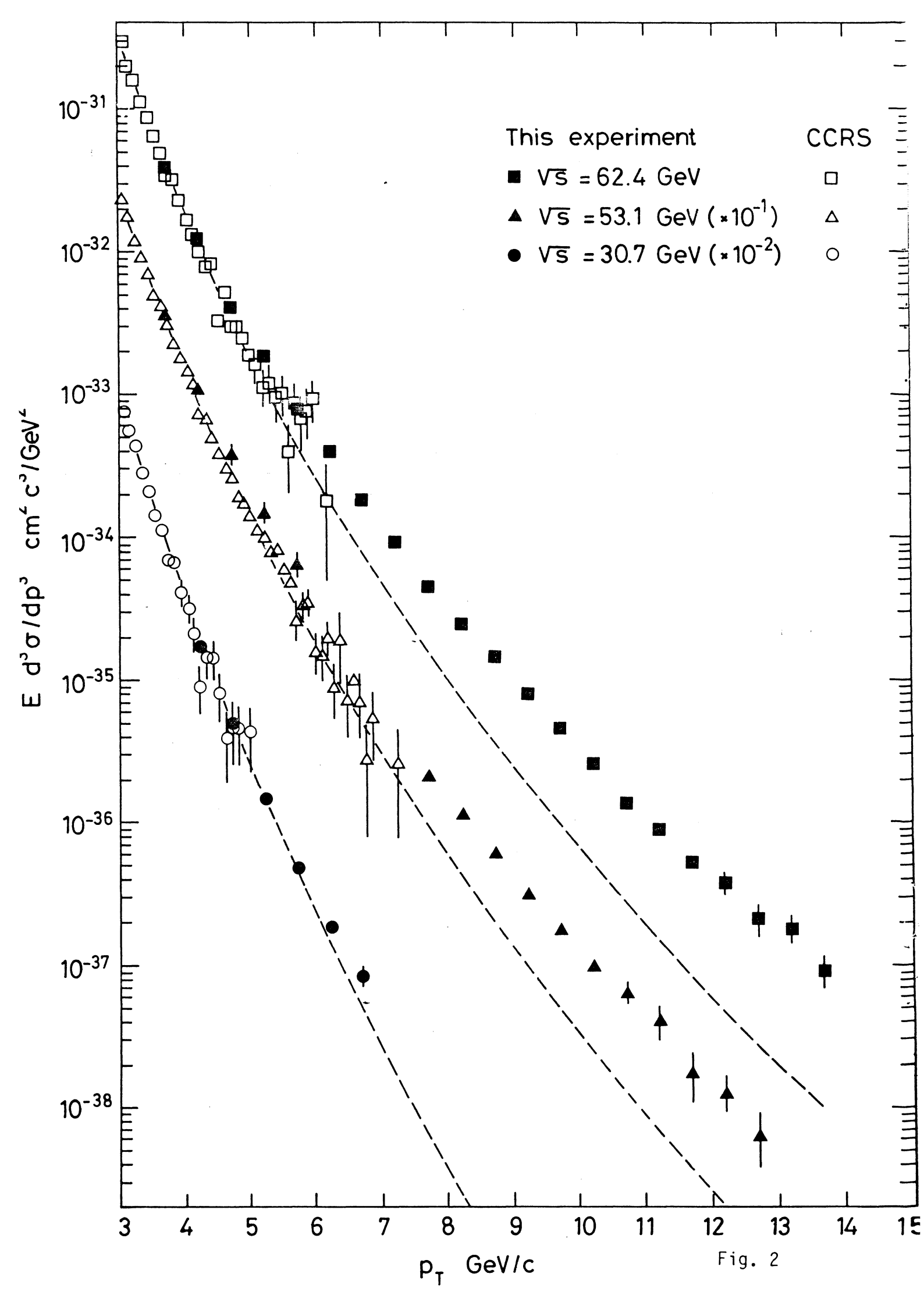
This experiment
CCRS
$\sqrt{s}$ = 62.4 GeV
$\sqrt{s}$ = 53.1 GeV (×10^{-1})
$\sqrt{s}$ = 30.7 GeV (×10^{-2})
E d$^3\sigma$/dp^3 cm^4 c^3/GeV^4
10^{-31}
10^{-32}
10^{-33}
10^{-34}
10^{-35}
10^{-36}
10^{-37}
10^{-38}
3
4
5
6
7
8
9
10
11
12
13
14
15
p_T GeV/c

Fig. 2

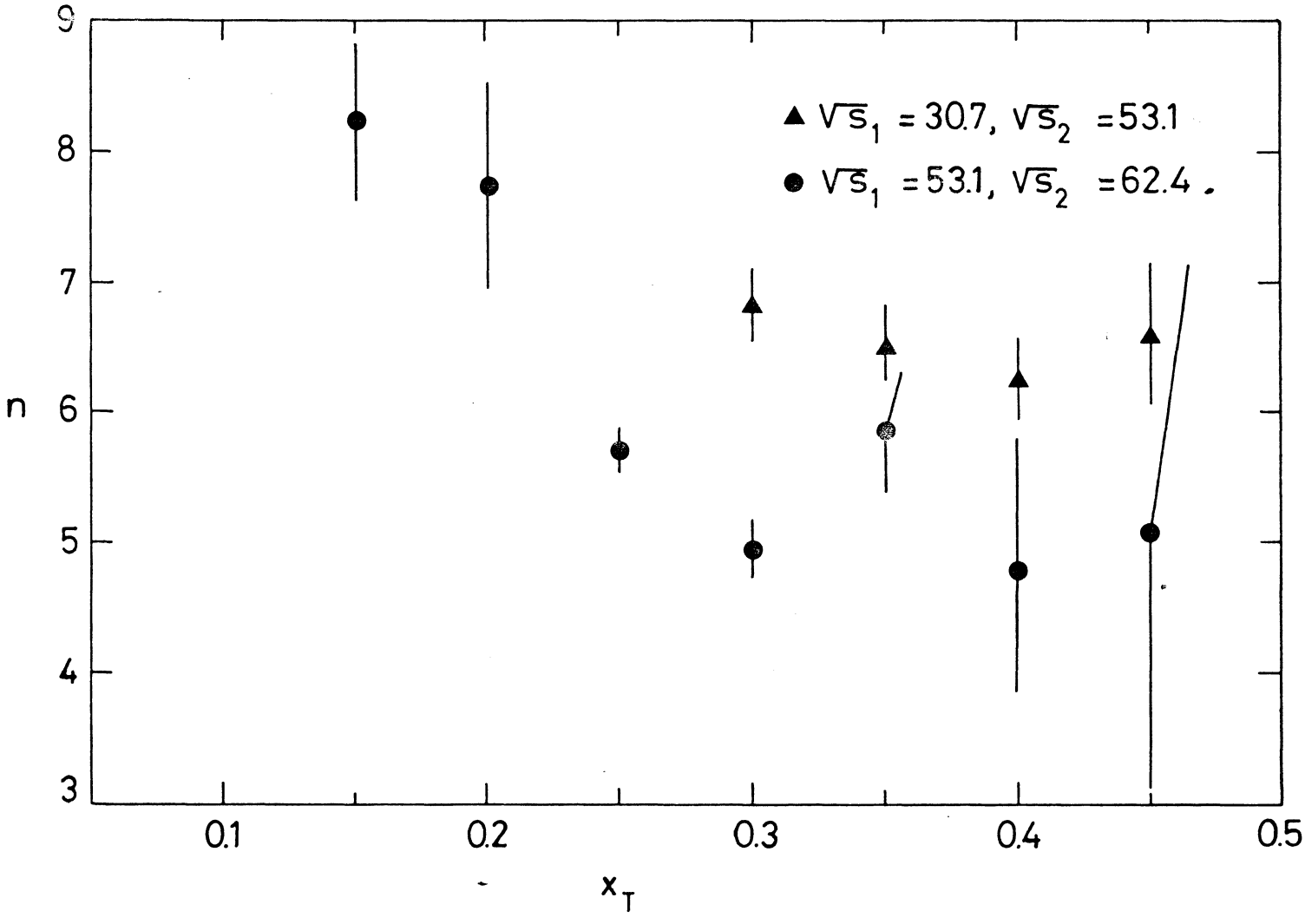
9
8
7
6
5
4
3
n
0.1
0.2
0.3
0.4
0.5
x_T
▲ $\sqrt{s}_1 = 30.7$, $\sqrt{s}_2 = 53.1$
● $\sqrt{s}_1 = 53.1$, $\sqrt{s}_2 = 62.4$

Fig. 3

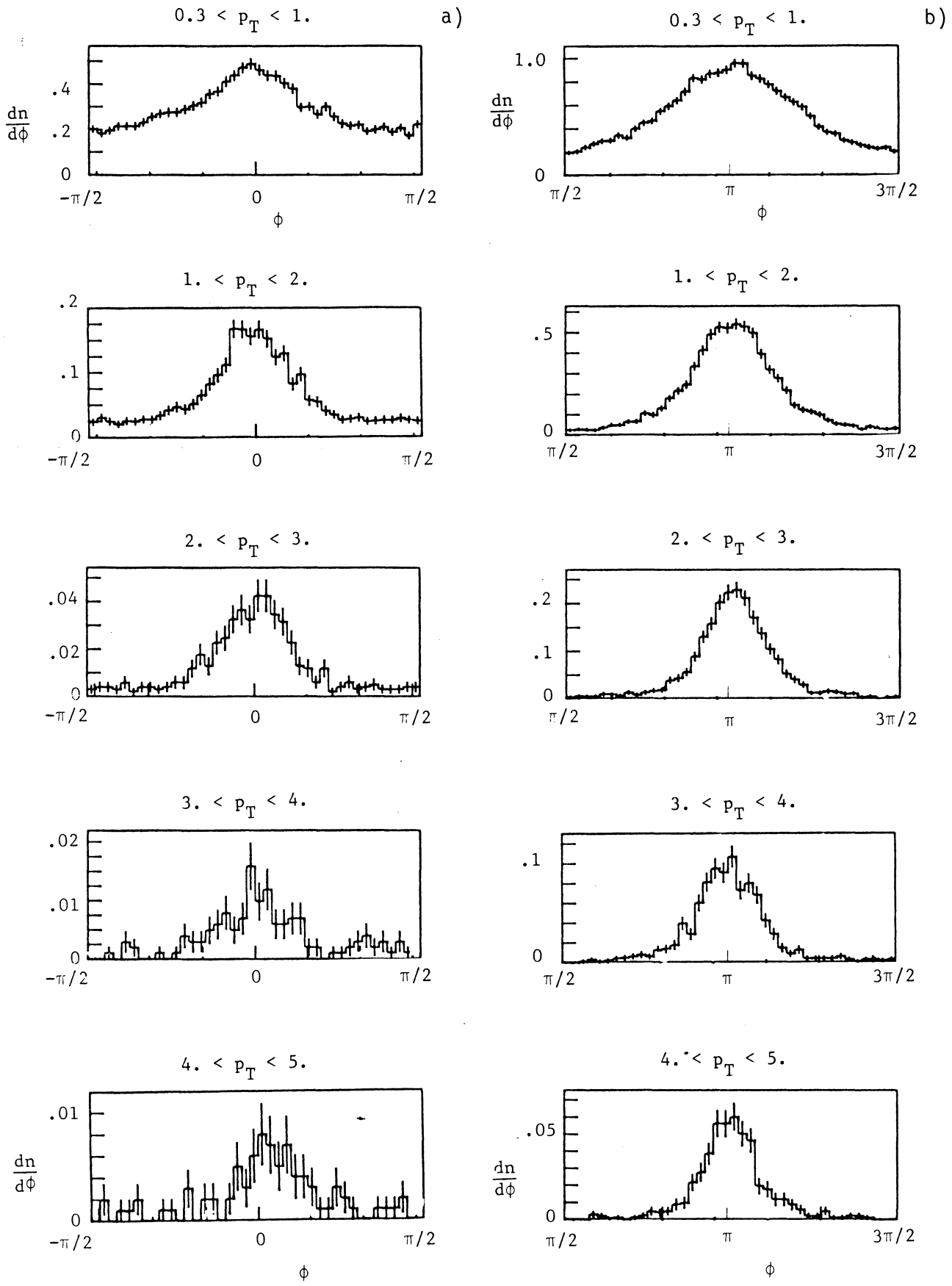

Fig. 4

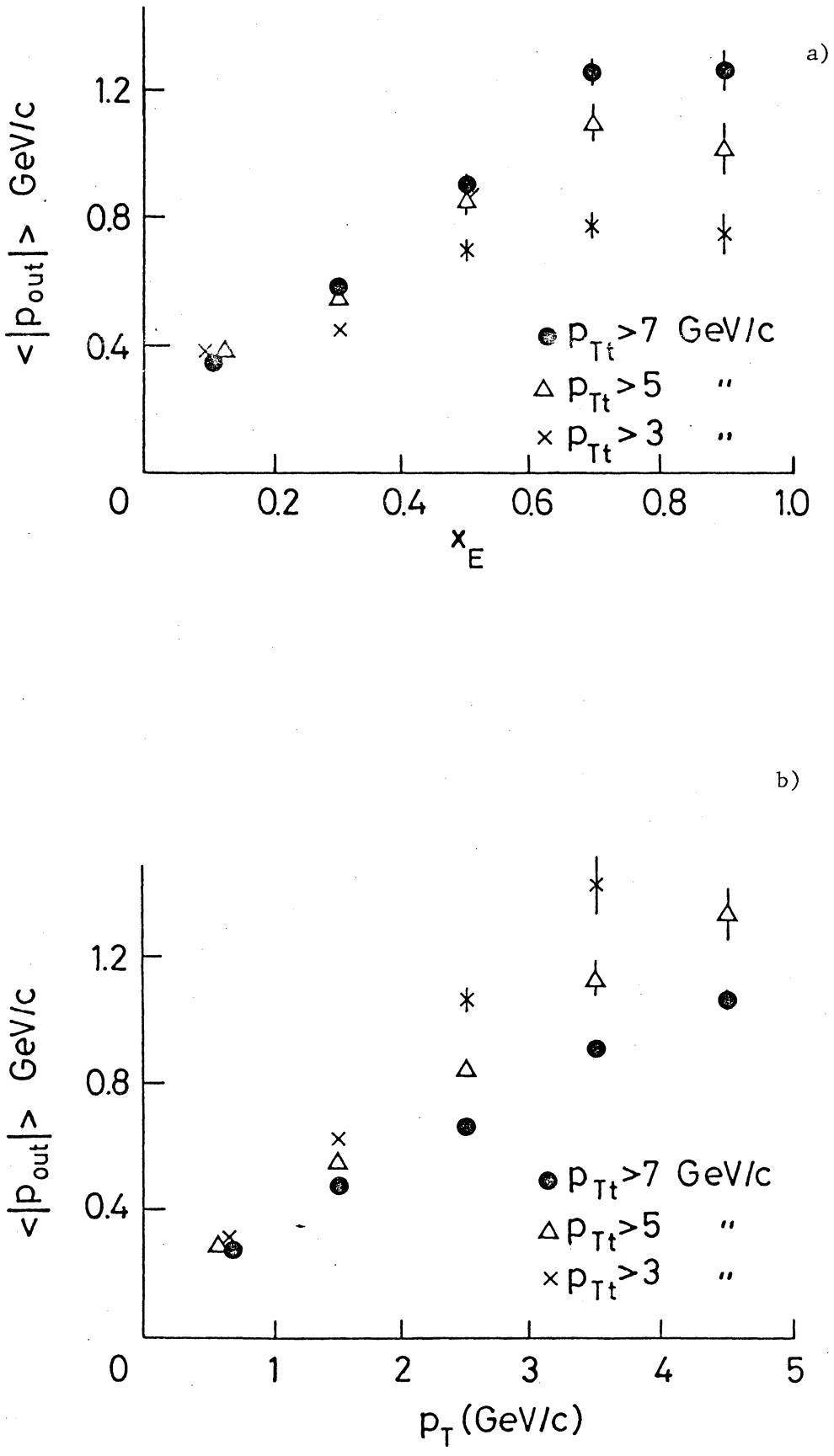
a)
1.2
0.8
0.4
0
0.2
0.4
0.6
0.8
1.0
x_E
$\langle|p_{out}|\rangle$ GeV/c
p_{Tt}>7 GeV/c
p_{Tt}>5 "
p_{Tt}>3 "
b)
1.2
0.8
0.4
0
1
2
3
4
5
p_T (GeV/c)
$\langle|p_{out}|\rangle$ GeV/c
p_{Tt}>7 GeV/c
p_{Tt}>5 "
p_{Tt}>3 "

Fig. 5

Fig. 6. Strip Chamber Hits
On Line.

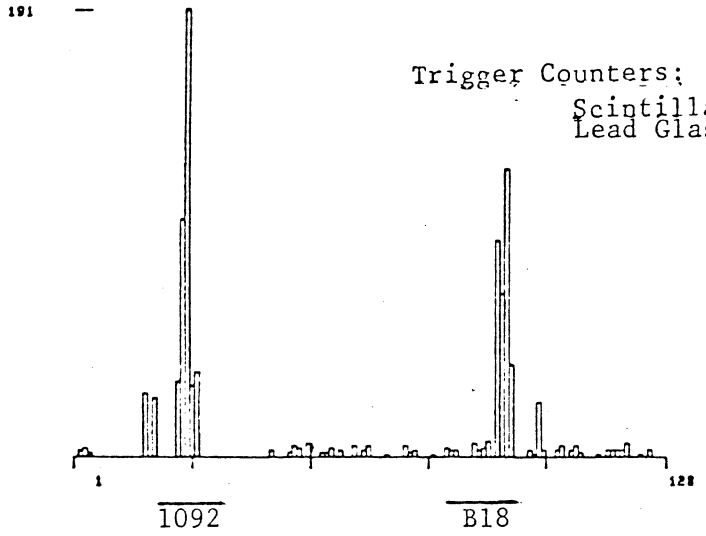

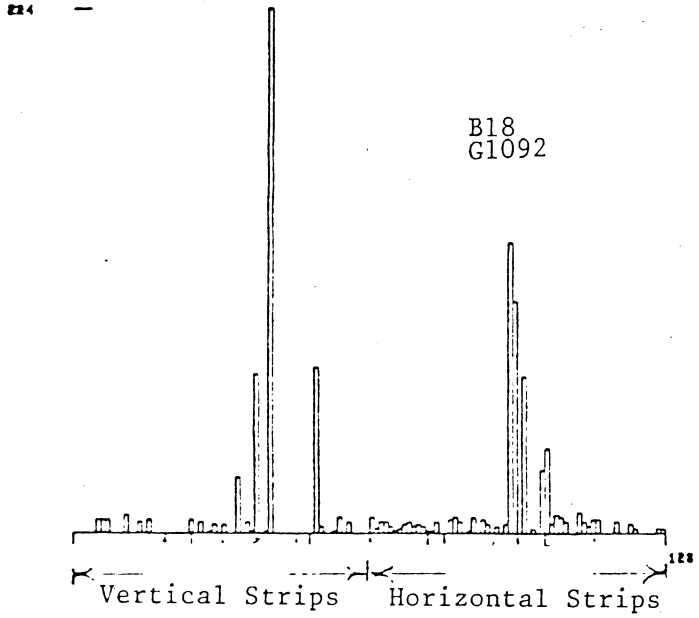

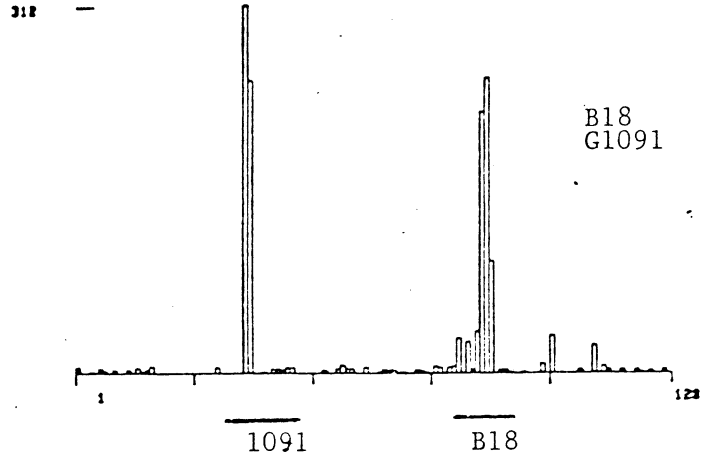

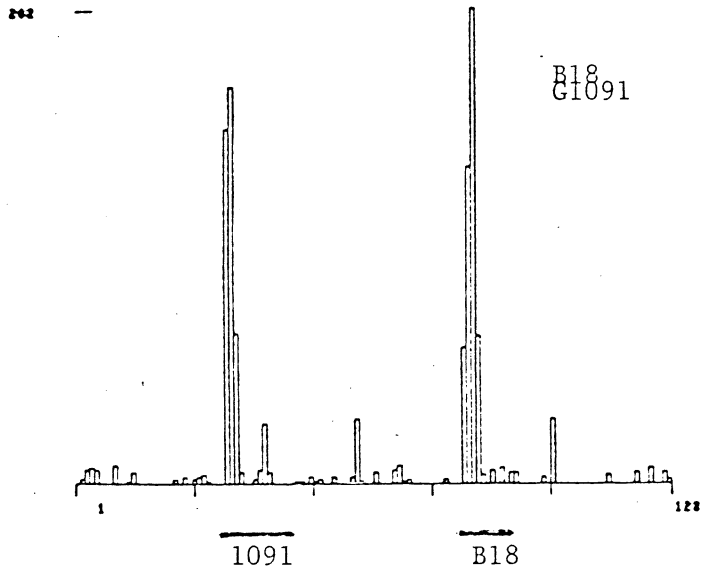

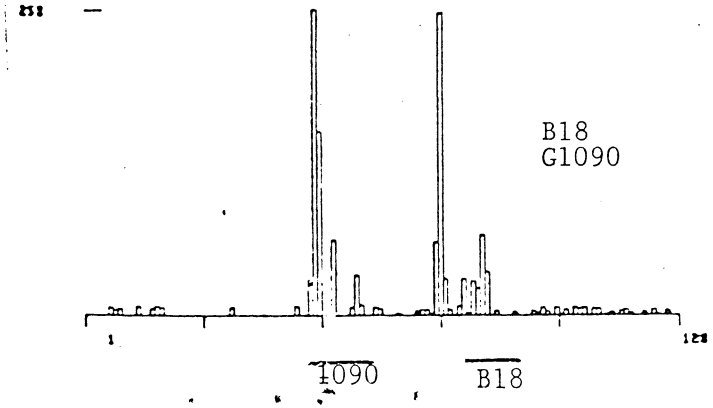

APPENDIX I

EUROPEAN ORGANIZATION FOR NUCLEAR RESEARCH

A STUDY OF HIGH MASS e^+e^- PAIRS PRODUCED IN p-p COLLISIONS AT THE CERN ISR

[CERN[1]-Columbia[2]-Oxford[3]-Rockefeller[4] (CCOR) Collaboration]

A.L.S. Angelis[3], B.J. Blumenfeld[2], L. Camilleri[1], T.J. Chapin[4], R.L. Cool[4], C. del Papa[1], L. Di Lella[1], Z. Dimčovski[4], R.J. Hollebeek[2], D. Levinthal[2], L.M. Lederman[2], J.T. Linnemann[4], L. Lyons[3], N. Phinney[3], B.G. Pope[1*], S.H. Pordes[1], A.F. Rothenberg[4**], A.M. Segar[3], J. Singh-Sidhu[1], A.M. Smith[1], M.J. Tannenbaum[4], R.A. Vidal[2***], J. Wallace-Hadrill[3], T.O. White[3†] and J.M. Yelton[3]

ABSTRACT

An apparatus consisting of a superconducting solenoidal magnet, cylindrical drift chambers, and two arrays of lead-glass Čerenkov counters has been used at the CERN ISR to study the production of e^+e^- pairs of invariant mass larger than 6 GeV/c^2.

Measurements of $(d^2\sigma/dmdy)_{y=0}$ for the e^+e^- continuum and of $B(d\sigma/dy)_{y=0}$ for the Υ resonances will be presented for $\sqrt{s}$ = 62.4 GeV. The mean p_T of the e^+e^- pairs and the multiplicity and momentum spectrum of associated particles will be discussed.

Geneva - 20 September 1978

Submitted to the
19th International Conference on High-Energy Physics,
Tokyo, August 1978

---

*) Present address: Physics Dept., Princeton University, New Jersey, USA.

**) Present address: CERN, Geneva, Switzerland.

***) Present address: Stanford Linear Accelerator Center, Stanford, Calif., USA.

†) Present address: Cavendish Laboratory, University of Cambridge, UK.

1. INTRODUCTION

The behaviour of the cross-section for the production of high-mass lepton pairs in pp collisions as a function of $\sqrt{s}$ is a topic of current interest. A measurement of the production cross-section of the recently discovered Υ resonances[1] as a function of $\sqrt{s}$ would shed light on the production mechanism involved. The large $\sqrt{s}$ available at the CERN Intersecting Storage Rings (ISR) makes it a suitable place for addressing these questions.

This paper presents data collected at the ISR on the production of electron pairs

$$p + p \rightarrow e^+ + e^- + X$$

at a c.m. energy of 62.4 GeV. The mass region covered is $m > 6$ GeV/c^2. Cross-sections in the form $(d^2\sigma/dmdy)_{y=0}$ and results on the mean transverse momentum $\langle p_T \rangle$ of the pairs and on the particles associated with the pairs are presented.

2. APPARATUS

The apparatus (Fig. 1) consists of a 1.5 tesla superconducting solenoid containing drift chambers, and of two lead-glass arrays located outside the magnet.

The solenoid coil is aluminium stabilized and has a thickness corresponding to one radiation length of aluminium. The inner dimensions of the solenoid are: radius = 70 cm, length = 170 cm. The field uniformity is ±1.5% over the volume of the drift chambers. The iron return yoke is built in such a way as to leave two windows obstructed only by the coil. Each window covers a laboratory angle of $45° < \theta < 135°$ and $90°$ in ϕ.

The drift chamber system[2] surrounds the vacuum pipe and consists of four modules DCM1-DCM4; each module contains two gaps. The sense wires run parallel to the magnetic field, and hence the drift times provide the ϕ coordinates of charged tracks. This is the coordinate that requires the highest accuracy because it is in the bending plane of the magnet. Delay lines are glued to the cathode planes facing each of the 580 sense wires. The times of arrival at the two ends

of the delay lines of the pulses induced on these delay lines give the z coordinate along the solenoid axis. The system thus provides pairs of ϕ, z coordinates, reducing off-line computer usage by eliminating the need for ϕ, z matching. Within a module, the sense wires of one gap are displaced with respect to the sense wires of the other gap by one half the sense-sense distance. This resolves most of the left/right sense wire ambiguities.

A lead-glass wall consisting of 168 blocks arranged in a 12 × 14 array is located behind each of the two windows in the solenoid. Each block has a cross-sectional area of 15 × 15 cm and is 40 cm thick (17 r.l.). The front face of each wall is located at 120 cm from the intersection region. To reduce the effect of the fringing field of the solenoid on the photomultipliers, a 6 mm thick iron plate is mounted on the front face of the arrays. Each block has been calibrated in an electron beam at the CERN Proton Synchrotron (PS). A small NaI crystal doped with ^{241}Am is glued to the front face of each block[3]. The pulse height of the light emitted by these crystals is recorded after every ISR run, thus providing a constant monitoring of this calibration. Two further checks on the calibration of each block are made:

i) the pulse-height spectrum resulting from the traversal of a block by hadrons is monitored;

ii) the lead-glass wall is positioned at 350 cm, and the π^0 mass is reconstructed from events where the two γ's are well separated.

It is estimated that the over-all absolute energy calibration is known to ±5%.

Two scintillator hodoscopes A and B are used. Hodoscope A, a "barrel" of 32 counters, is mounted between DCM1 and DCM2. It is used to provide, event by event, a zero time relative to which the drift chamber times are measured. Hodoscope B is mounted against the outer face of the coil and consists of one 12-counter array in front of each of the two thin windows of the solenoid. In this analysis it was used to measure the number of particles emerging from the coil along the electron candidate track. All A and B scintillators are equipped with photomultipliers at both ends, and the pulse heights from all phototubes are recorded.

The stainless-steel vacuum pipe has an average thickness of 0.36 mm (0.02 radiation lengths).

3. TRIGGER

For the electron pair experiment the detector was triggered by the deposition of more than 2 GeV of energy in each of the two lead-glass arrays. The energy in each array was further constrained by hardware to consist of at least 1.5 GeV in three adjacent columns and 1.5 GeV in three adjacent rows. Finally, the on-line software required that at least 1.5 GeV be recorded in a 3 × 3 block cluster. The cluster requirement was designed to reject events in which the energy in an array was due to several particles, The trigger did not include a charged particle requirement and was therefore sensitive to $\pi^0\pi^0$ pairs, which constitute the vast majority of the recorded events.

A trigger rate of 2-3/sec was the maximum consistent with off-line computer time availability. At the average luminosity of $\sim 3 \times 10^{31}$ cm^{-2} sec^{-1} at which these data were collected, this constraint dictated the level of the thresholds described above.

4. ANALYSIS AND CUTS

As explained in the previous section, the majority of the triggers consisted of $\pi^0\pi^0$ pairs. The first step in the data reduction was therefore to require a track coming from the intersection region to point within 12 cm of the centre of gravity of a 3 × 3 block energy-cluster in the lead glass. One such electron candidate was required in each array. The remaining events included electron pairs plus a background arising from

i) charged hadrons depositing most of their energy in the lead glass by interacting in the coil or in the glass itself;

ii) Dalitz decays and γ-ray conversions in the vacuum pipe and part of DCM1;

iii) spatial overlaps of a π^0 providing the energy deposition in the lead glass, with a charged hadron providing the track.

Energy deposition from all these sources of background tends to be more spread out in space than that from an electron. To make use of this fact, the energy of the cluster was estimated in two ways. A measure of the energy E_9 was obtained by summing the nine blocks in the 3 × 3 block cluster. A second measure E_c was obtained by summing only those blocks intersected by a truncated cone with the track as its axis and with radii of 3 cm at the front face of the glass and 7.5 cm at a distance of 40 cm into the glass, as measured along the track. The ratio $RC = E_c/E_9$ is plotted in Fig. 2 for events where the two candidate tracks have opposite charge and for events where they have the same charge. This ratio was required to be greater than 0.98.

The majority of hadrons traverse the coil without interacting and give a pulse height in the B counter equivalent to single ionization (s.i.). Electrons, on the other hand, shower in the coil and give large pulse heights. One or the other of the two candidate electrons of a pair was required to have a pulse height in the B counter greater than 1.5 s.i. A charged hadron has a 35% probability of having a pulse height greater than 1.5 s.i., whereas an electron has a 78% probability.

In order to reject conversions in the A counters and the second half of DCM1 (0.025 radiation lengths in total), the candidate track was required to have at least one hit in DCM1.

In some cases both members of a conversion pair (internal or external) were seen in the drift chambers. To reject these events, the effective mass of the candidate track with each of the other tracks in the event was formed in turn, assuming both particles were electrons. The distribution of these masses is shown in Fig. 3 for combinations where the second track has the opposite and the same charge as the candidate track. The plots have the same shape down to 150 MeV/c^2 in mass. Below this mass the events are predominantly of opposite charge. This difference is attributed to Dalitz decays and conversions. Candidate electrons were therefore rejected if they formed a mass of less than 150 MeV/c^2 with an associated track of opposite charge.

A characteristic of an electron is that its momentum p, as measured by the drift chambers, must equal the energy E, as measured by the lead glass within the accuracy of the two measurements. The energy as measured in the lead glass E_{obs} was corrected for energy loss in the coil and iron plate, assuming the observed particle was an electron. The following algorithm, developed during a study of the coil-B counter-glass response in a PS test beam, was used. The average correction applied was 0.28 GeV:

$$E = E_{obs} + 0.080 + 0.015\ E_{obs} + 0.024(PHB - 2.5)$$

where E_{obs} is in GeV, and PHB is the pulse height in the B counter in units of s.i. The r.m.s. energy resolution of the lead glass is given by $\Delta E/E = 0.05 + 0.07/\sqrt{E}$, whereas the r.m.s. momentum resolution of the drift chamber/solenoid system is $\Delta p/p \sim 0.07\ p$. The quantity E/p was computed for each candidate track. Electrons arising from conversion have $E/p > 1.0$ since the electron carries only a fraction of the π^0 energy and one electron is measured by the chambers to give p. On the other hand, the two gamma rays from a background π^0 merge in our apparatus into a single cluster. The energy measured by the lead glass is therefore that of the whole π^0. The majority of overlaps also have $E/p > 1.0$ since in general the overlapping track is of low momentum. On the other hand, charged hadrons satisfying the trigger requirements tend to have E/p equal to or slightly smaller than 1.0. The higher the momentum of the hadron the larger is the probability of depositing a given amount of energy in the lead glass. However, this is outweighed by the fact that the p_T spectrum of hadrons is falling steeply. It is therefore those hadrons depositing most of their energy in the lead glass that are the main source of background. A plot of E/p for opposite charge and same charge events is shown in Fig. 4. For each candidate electron the uncertainty σ_{Ep} on E/p arising from the measurement on E and p was computed, and the candidate particle was retained if the measured E/p was in the range

$$0 < E/p < 1 + 2\ \sigma_{Ep}\ .$$

5. RESULTS

Data corresponding to an integrated luminosity = 3.5×10^{37} cm^{-2} sec^{-1} have been analysed to date. Application of the above cuts resulted in 81 candidate pairs of opposite charge and 24 of same charge. The mass was calculated using the lead-glass energy. The resulting distributions are shown in Fig. 5. The drop below 6 GeV/c^2 is because of trigger thresholds. The background in the opposite sign pairs was assumed to be equal to the same charge pairs. A bin-by-bin subtraction can then be performed, and the cross-section was computed using

ρ = geometrical acceptance derived from Monte Carlo calculation assuming the production is flat in rapidity over the apparatus ($|y| < 0.7$), = 0.10;

ε_{CH} = track reconstruction efficiency = 0.90 per track;

ε_{B} = efficiency of B counter cut = 0.95 per pair;

ε_{Ep} = efficiency of E/p cut = 0.98 per track;

ε_{RC} = efficiency of RC cut = 0.90 per track;

ε_{D} = efficiency of Dalitz and conversion cut. The only inefficiency would arise from the accidental vetoing of a genuine electron by an associated track. Only 10% of the events were removed by this cut, and it lost the same number of same and opposite charge pairs; ε_{D} was therefore taken to be 1.0.

The cross-sections $(d^2\sigma/dmdy)_{y=0}$ are tabulated in Table 1 together with the number of events and background events. The cross-sections are shown in Fig. 6 together with the data obtained at $\sqrt{s}$ = 62.4 GeV by another ISR experiment[4]. A fit derived from Fermilab data[1] and scaled to $\sqrt{s}$ = 62.4 GeV according to the scaling law $d\sigma/dm = (1/m^3)f(m/\sqrt{s})$ is also shown in Fig. 6 and is in very good agreement with the data.

Given the reported masses of the three Υ peaks[5] and the energy resolution of this experiment [Δm (FWHM) = 1.25 GeV/c^2], the Υ region is defined as 8.75 GeV/c^2 to 11.0 GeV/c^2. Assuming all 15 events in this mass interval to be due to the Υ,

$$B \left.\frac{d\sigma}{dy}\right|_{y=0} = (7.8 \pm 2.0) \times 10^{-36} \text{ cm}^2$$

or a factor of 30 ± 8 larger than the Fermilab result at $\sqrt{s}$ = 27.4 GeV. Although the geometrical acceptance of the apparatus increases with mass and the experiment is sensitive to masses up to 60 GeV/c^2, no event was observed above 13 GeV/c^2.

The p_T distributions for the e^+e^- candidates and for the background are shown in Fig. 7 for two mass intervals:

i) 6-8.75 GeV/c^2

ii) > 8.75 GeV/c^2 .

After subtraction of the background, the mean p_T is found to be

$$1.67 \pm 0.21 \quad \text{and} \quad 1.65 \pm 0.20 \text{ GeV/c}$$

for the two mass intervals. These values are to be compared to a mean p_T of 1.2 GeV/c obtained at Fermilab[6] for 6 < m < 8 GeV/c^2 at $\sqrt{s}$ = 27.4 GeV. These values of the mean p_T can also be compared with the mean p_T of the $\pi^0\pi^0$ pairs in the same mass intervals, 2.1 ± 0.1 and 2.3 ± 0.1 GeV/c, respectively.

Since the drift chamber system has a large acceptance ($\Delta\phi$ = 360° and $\Delta\theta$ = = 90° ± 45°) it was possible to measure the momentum spectrum and mean multiplicity of the tracks associated with the e^+e^- candidates. The transverse momentum spectra of positive and negative tracks are very similar and were therefore combined. This combined spectrum is shown in Fig. 8 for the two mass intervals described earlier. The transverse momentum spectra for tracks associated with $\pi^0\pi^0$ events with effective mass in the same two mass intervals are also shown. The three spectra are normalized in the bin 0.25-0.50 GeV/c. The spectra for the tracks associated with e^+e^- events appears to be steeper than the spectra for the tracks associated with $\pi^0\pi^0$ events.

The mean multiplicity of tracks associated with e^+e^- events is 6.1 ± 1.0 and 5.5 ± 1.0 for the two mass intervals, to be compared with 10.0 ± 0.2 and 9.5 ± 0.3 for $\pi^0\pi^0$ events.

REFERENCES

1) S.W. Herb et al., Phys. Rev. Letters 39 (1977) 252.

2) L. Camilleri et al., presented at the Wire Chamber Conference, Vienna, 1978, Proc. to be published in Nuclear Instrum. Methods.

3) J.S. Beale et al., Nuclear Instrum. Methods 117 (1974) 50.

4) J.H. Cobb et al., Phys. Letters 72 (1977) 273.

5) L.M. Lederman, Proc. Internat. Symposium on Lepton and Photon Interactions at High Energies, Hamburg, 1977 (DESY, Hamburg, 1977), p. 567.

6) D.M. Kaplan et al., Phys. Rev. Letters 40 (1978) 435.

Table 1

Mass (GeV/c^2)	Number of events: Opposite sign	Number of events: Same sign	Signal	τ ($m/\sqrt{s}$)	$(d^2\sigma/dmdy)_{y=0}$ ($cm^2/GeV/c^2$)
6.0-6.5	24	7	17 ± 5.6	0.100	$(1.8 \pm 0.6) \times 10^{-35}$
6.5-7.0	14	5	9 ± 4.3	0.108	$(9.4 \pm 4.5) \times 10^{-36}$
7.0-8.0	15	9	6 ± 5.0	0.120	$(3.1 \pm 2.5) \times 10^{-36}$
8.0-9.0	7	2	5 ± 3.0	0.136	$(2.6 \pm 1.6) \times 10^{-36}$
9.0-9.5	10	0	10 ± 3.2	0.148	$(1.0 \pm 0.33) \times 10^{-35}$
9.5-10.0	3	0	3 ± 1.7	0.156	$(3.1 \pm 1.8) \times 10^{-36}$
10.0-11.0	1	0	1 ± 1	0.168	$(2.0 \pm 2.0) \times 10^{-36}$
11.0-12.0	1	0	1 ± 1	0.184	$(2.0 \pm 2.0) \times 10^{-36}$

Figure captions

Fig. 1 : a) The apparatus as viewed along the solenoid axis.

b) Top view of the apparatus.

Fig. 2 : The ratio RC, as defined in the text, plotted for opposite charge and same charge electron pair candidates.

Fig. 3 : Effective mass of candidate electrons with each of the other particles in the event. The distribution for combinations in which the other particle is of opposite charge to that of the candidate is plotted separately from the distribution in which the other particle is of same charge.

Fig. 4 : The quantity E/p, defined in the text, plotted for opposite charge and same charge electron pair candidates.

Fig. 5 : Mass distribution of opposite charge and same charge electron pair candidates.

Fig. 6 : Differential cross-sections at y = 0, for e^+e^- production at $\sqrt{s}$ = 62.4 GeV. The background has been subtracted.

Fig. 7 : Distribution of the p_T of the e^+e^- candidates. The distributions are shown for candidates of opposite and same charge and for two mass intervals

i) $6 < m_{ee} < 8.75$ GeV/c^2

ii) $m_{ee} < 8.75$ GeV/c^2.

Fig. 8 : The transverse momentum spectrum of particles associated with

a) e^+e^- pairs

b) $\pi^0\pi^0$ pairs.

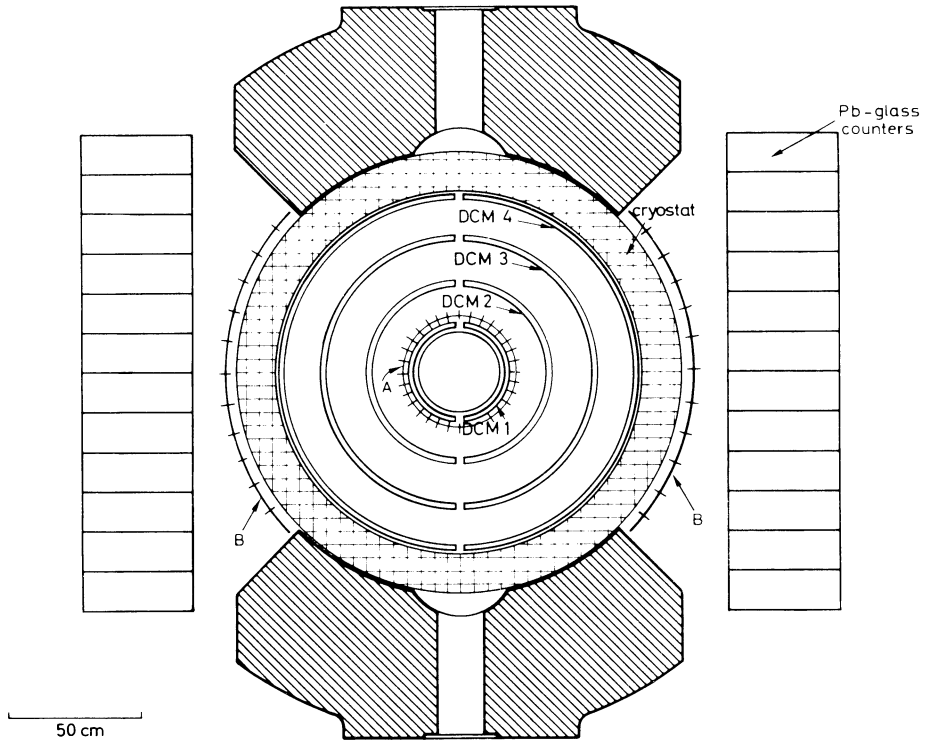
a)
Pb-glass
counters
cryostat
DCM 4
DCM 3
DCM 2
DCM 1
A
B
B
50 cm

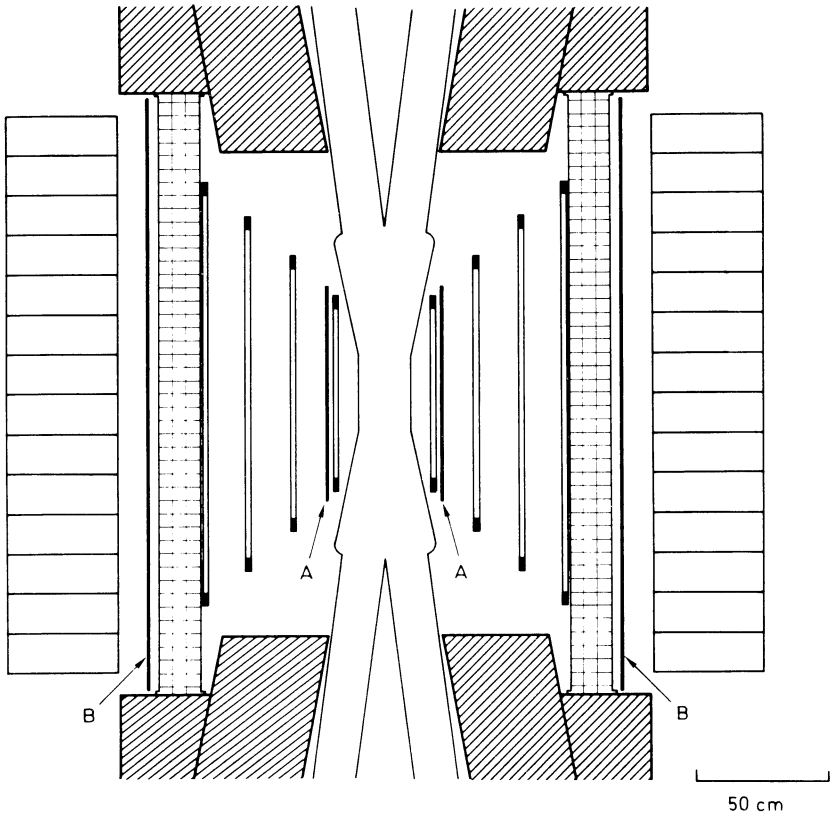
b)
A
A
B
B
50 cm

Fig. 1

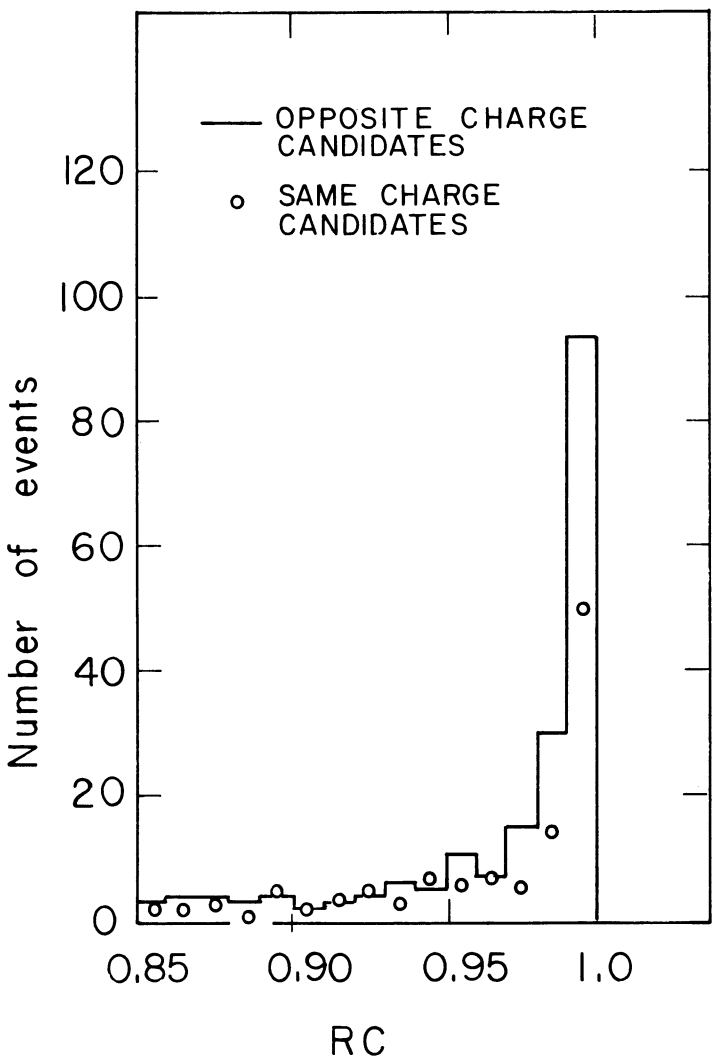
OPPOSITE CHARGE CANDIDATES
SAME CHARGE CANDIDATES
Number of events
120
100
80
60
40
20
0
0.85
0.90
0.95
1.0
RC

Fig. 2

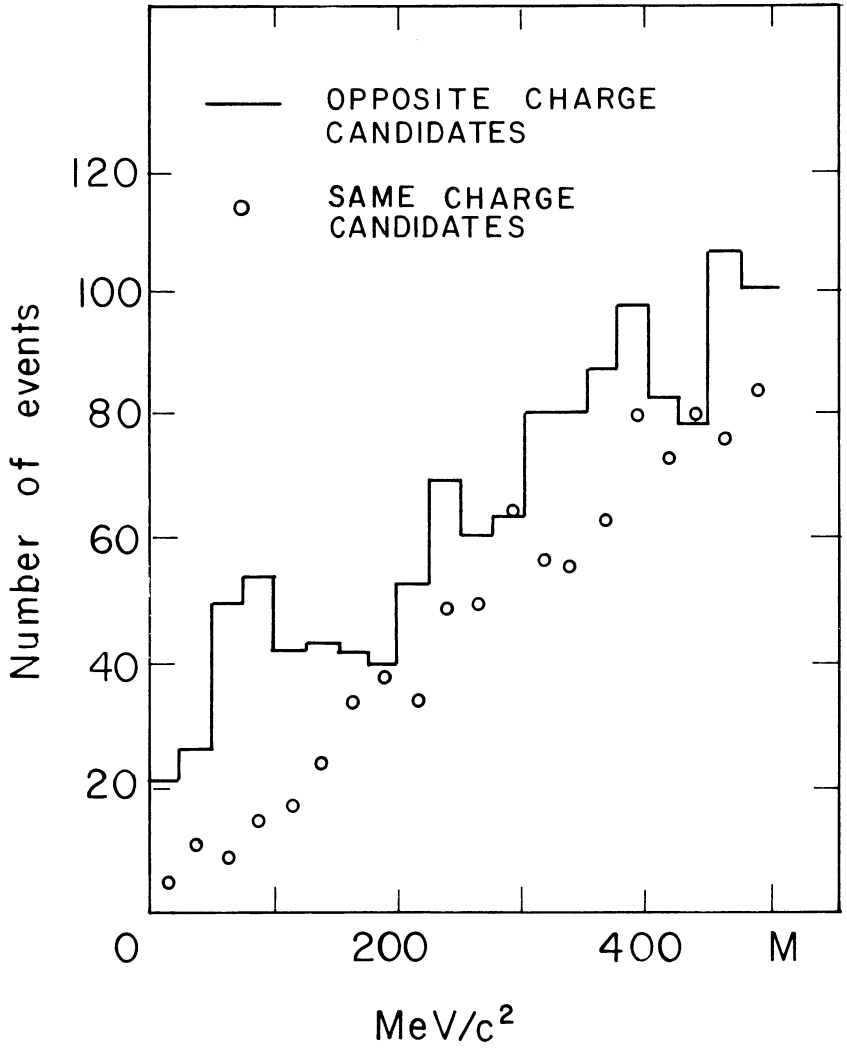
OPPOSITE CHARGE CANDIDATES
SAME CHARGE CANDIDATES
Number of events
120
100
80
60
40
20
0
200
400
M
MeV/c²

Fig. 3

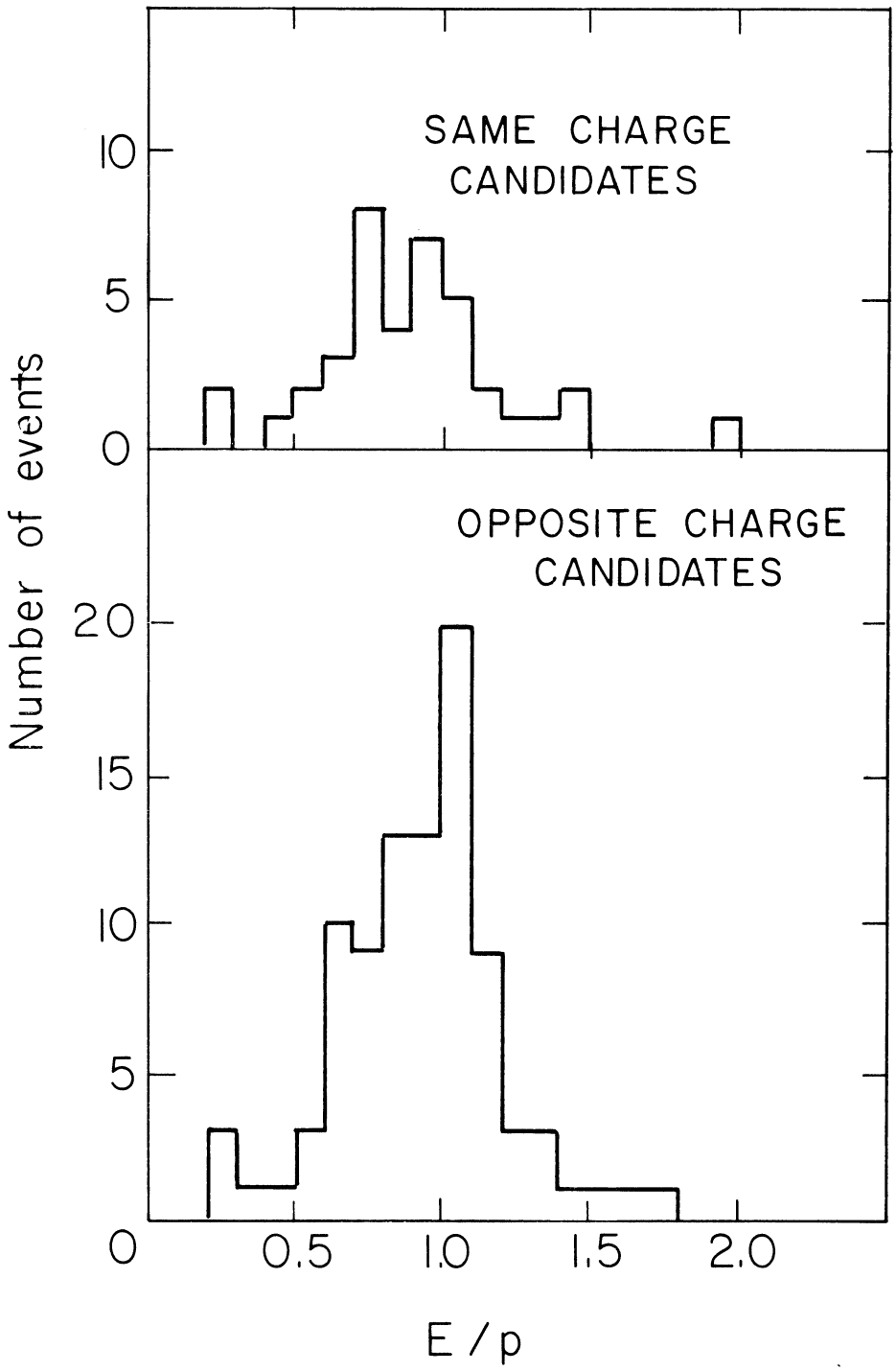
SAME CHARGE
CANDIDATES
OPPOSITE CHARGE
CANDIDATES
Number of events
10
5
0
20
15
10
5
0
0.5
1.0
1.5
2.0
E / p

Fig. 4

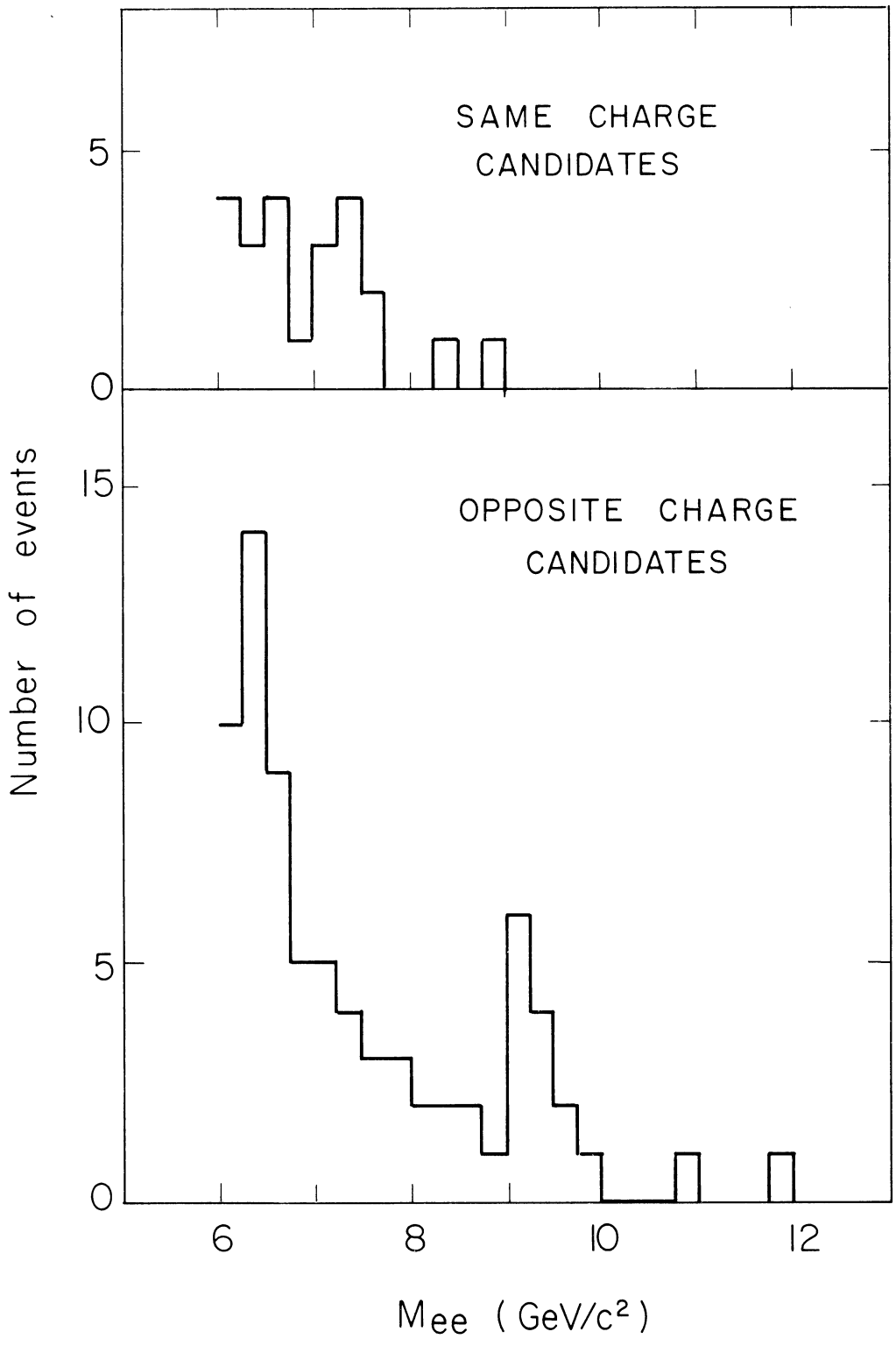
SAME CHARGE
CANDIDATES
OPPOSITE CHARGE
CANDIDATES
Number of events
5
0
15
10
5
0
6
8
10
12
Mee (GeV/c²)

Fig. 5

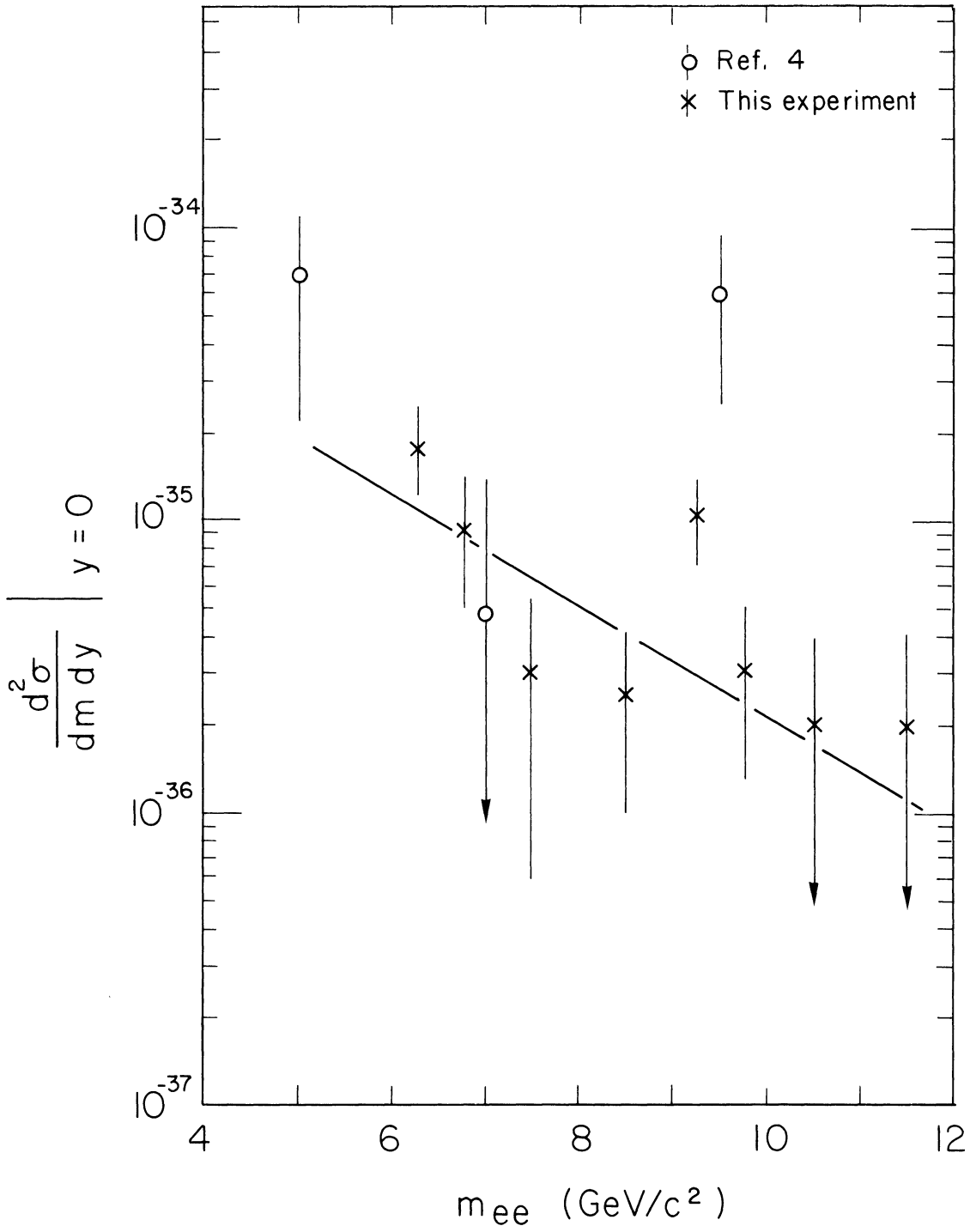
Ref. 4
This experiment
10^{-34}
10^{-35}
10^{-36}
10^{-37}
$\frac{d^2\sigma}{dm\,dy}\Big|_{y=0}$
4
6
8
10
12
m_{ee} (GeV/c^2)

Fig. 6

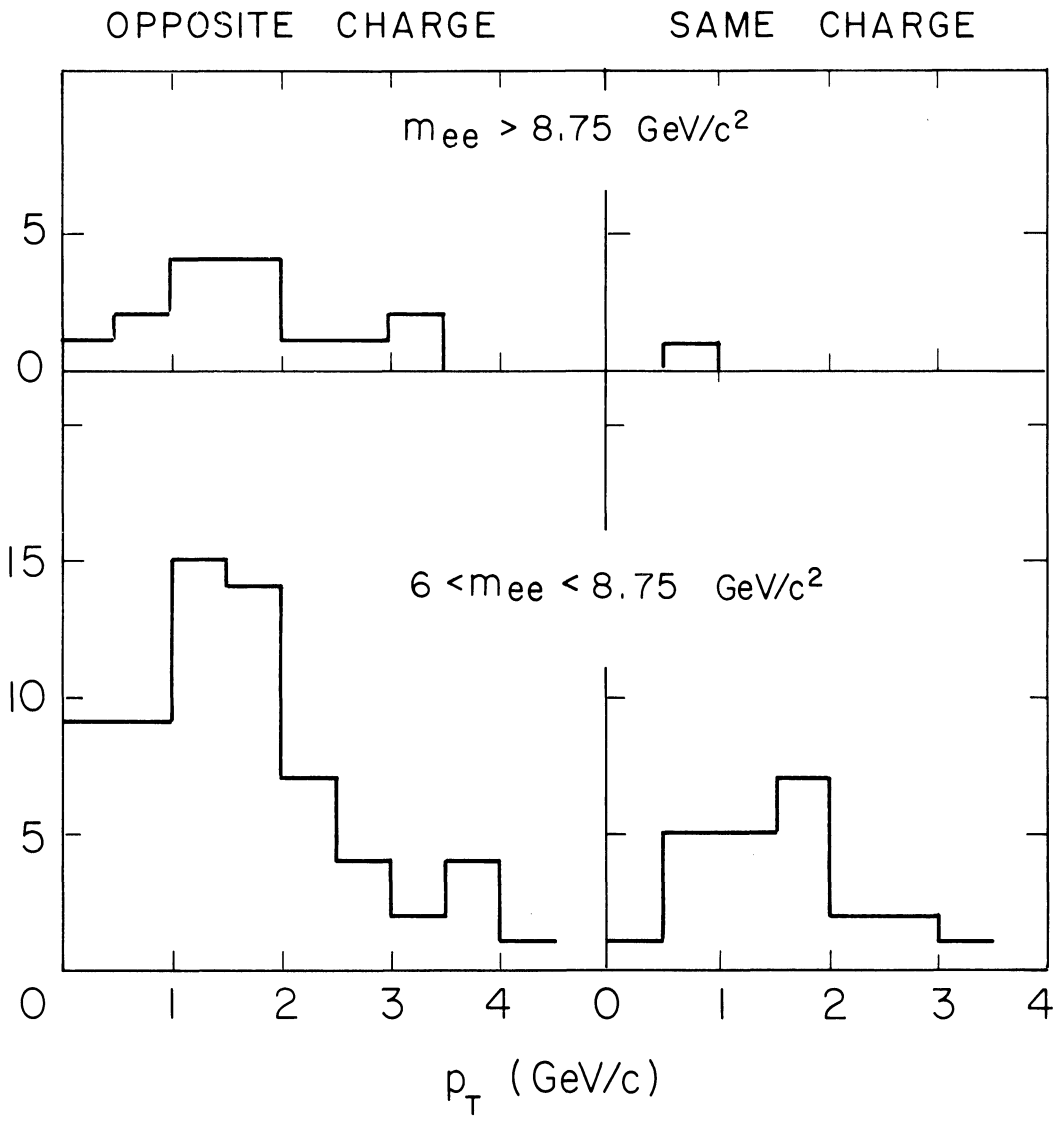
OPPOSITE CHARGE
SAME CHARGE
$m_{ee} > 8.75$ GeV/c^2
$6 < m_{ee} < 8.75$ GeV/c^2
5
0
15
10
5
0
1
2
3
4
0
1
2
3
4
p_T (GeV/c)

Fig. 7

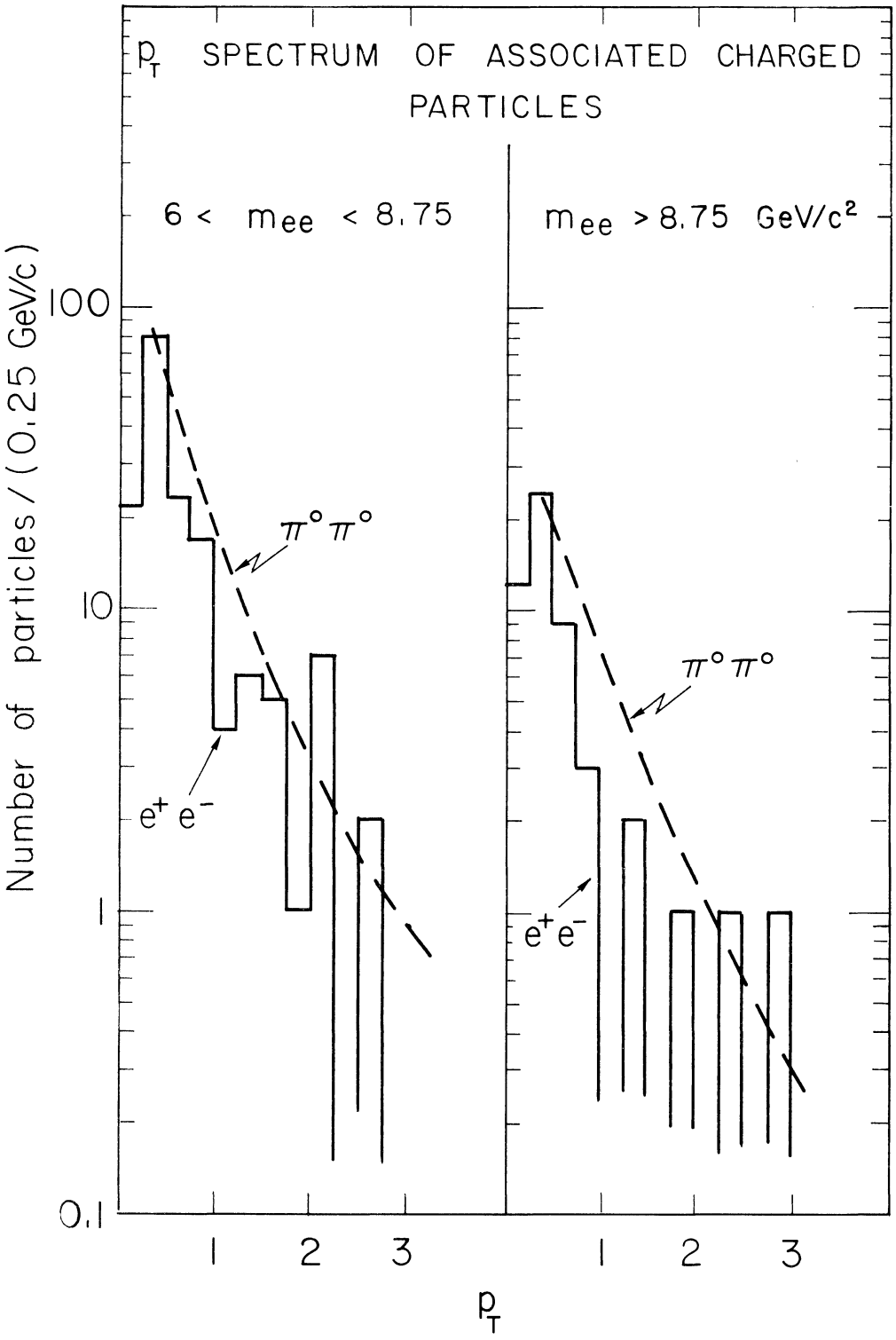
p_T SPECTRUM OF ASSOCIATED CHARGED PARTICLES
6 < m_{ee} < 8.75
m_{ee} > 8.75 GeV/c^2
Number of particles / (0.25 GeV/c)
100
10
1
0.1
$\pi^0\pi^0$
e^+e^-
$\pi^0\pi^0$
e^+e^-
1
2
3
1
2
3
p_T

Fig. 8

APPENDIX II

EUROPEAN ORGANIZATION FOR NUCLEAR RESEARCH

A Measurement of Inclusive π^0 Production at Large p_T from p-p Collisions at the CERN ISR

CERN-Columbia-Oxford-Rockefeller (CCOR) Collaboration

A.L.S. Angelis[c], B.J. Blumenfeld[b], L. Camilleri[a], T.J. Chapin[d], R.L. Cool[d], C. del Papa[a], L. Di Lella[a], Z. Dimčovski[d], R.J. Hollebeek[b], L.M. Lederman[b], D. Levinthal[b], J.T. Linnemann[d], L. Lyons[c], N. Phinney[c], B.G. Pope[a,1], S.H. Pordes[a], A.F. Rothenberg[d,2], A.M. Segar[c], J. Singh-Sidhu[a], A.M. Smith[a], M.J. Tannenbaum[d], R.A. Vidal[b,3], J. Wallace-Hadrill[c], T.O. White[c,4] and J.M. Yelton[c].

a CERN, Geneva, Switzerland

b Columbia University, New York, NY, USA[5]

c University of Oxford, Oxford, UK.

d The Rockefeller University, New York, NY, USA[6]

ABSTRACT

The inclusive cross-section for large p_T π^0 production near 90^o in p-p collisions at the CERN ISR is presented for centre-of-mass energies 30.7, 53.1 and 62.4 GeV. The data are inconsistent with scaling of the form $p_T^{-n} F(x_T)$, with constant n or with n allowed to depend on $x_T = 2p_T/\sqrt{s}$. For $\sqrt{s}$ = 53.1 and 62.4 GeV, the value of n found for $3.5 < p_T < 7.0$ GeV/c is $n = 8.0 \pm 0.5$, in agreement with previous experiments. However, for $7.5 < p_T < 14.0$ GeV/c the value becomes $n = 5.1 \pm 0.4$.

Submitted to Physics Letters

September 1978

---

1 Present address : Physics Dept., Princeton University, Princeton, USA.

2 Present address : CERN, Geneva, Switzerland.

3 Present address : Stanford Linear Acc. Center, Stanford, CA, USA.

4 Present address : Cavendish Laboratory, University of Cambridge, Cambridge, UK.

5 Research supported in part by the National Science Foundation

6 Research supported in part by the Department of Energy.

The production of high p_T secondaries from hadron collisions at high energy has been the subject of extensive studies in the last few years, both at the CERN ISR [1-6] and at Fermilab [7-9]. Measurements of inclusive pion production up to transverse momenta $p_T \sim 8$ GeV/c for various values of the total centre-of-mass energy $\sqrt{s}$, showed that the invariant cross-section around 90^o could be described by the scaling form [10,11]

$$E \frac{d^3\sigma}{dp^3} = p_T^{-n} F(2p_T/\sqrt{s}) \qquad (1)$$

with $n \sim 8$ [4]. Recent theoretical work [12] based on QCD predicts that the scaling form (1) is not valid, and that the invariant cross-section should approach the p_T^{-4} law as p_T is increased at a fixed value of $x_T = 2p_T/\sqrt{s}$.

We report here the results of an experiment on inclusive π^0 production from p-p collisions at the CERN ISR, in which π^0's have been measured around 90^o over the p_T range 3.5 to 14 GeV/c, at the $\sqrt{s}$ values 30.7, 53.1 and 62.4 GeV. The experimental apparatus (Fig. 1) consisted of two arrays of lead glass Čerenkov counters, on either side of a superconducting solenoid, at a distance of 1.40 m from the interaction point. The solenoid provided a magnetic field of 1.5 T over a cylindrical volume 1.40 m in diameter and 1.7 m long. A hodoscope of 32 scintillation counters (A), and four double gap cylindrical drift chamber modules with two-dimensional readout (DCM1-DCM4) located in the magnetic field measured the momenta of any charged particles produced. Two hodoscopes of 12 scintillation counters (B) were just outside the solenoid, against the external shell of the cryostat. The total thickness of the cryostat and coil together was 23 g/cm^2 (mainly aluminium) corresponding to 1.0 radiation length. Each lead glass array was composed of 168 blocks, 15 x 15 x 40 cm^3 corresponding to 17 radiation lengths, arranged in 12 rows of 14. A 0.3 cm thick iron plate in front of each array was used for magnetic shielding. Details of the magnet [13] and chambers [14] have been given elsewhere.

The lead glass counters were calibrated individually in an electron beam of known energy at the CERN PS. In order to monitor the stability of the calibration, each counter was equipped with a light pulser [15] consisting

of a NaI(Tl) crystal doped with ^{241}Am, and the resulting pulse height spectrum was recorded every two days. Because of the deterioration of many of these pulsers, and as an additional check, the lead glass arrays were withdrawn once a month to a distance of 3.5 m from the interaction region in order to measure the pulse height spectrum produced by penetrating charged particles (a $\sim$ 20% FWHM peak, at an energy of about 0.5 GeV). In the withdrawn position, a further check on the energy calibration was provided by events containing two spatially resolved photons, for which the π^0 mass could be measured directly. The variation of individual blocks from the average energy calibration was 5% r.m.s; and the uncertainty in the absolute energy scale was $\pm$ 5%.

A trigger was generated whenever the sum of the 168 signals from either lead glass array exceeded a given threshold, in coincidence with a signal from any of the A counters. The integrated luminosities for the thresholds and $\sqrt{s}$ values used are listed in Table I. Data taking for the various conditions was interleaved to minimize systematic effects. The luminosity was monitored by two pairs of counter telescopes located near the B hodoscope, and calibrated by the Van der Meer method [16]. At the typical luminosity of $2 \times 10^{31} cm^{-2} sec^{-1}$, the triggering rate was $\sim$ 1 per second at the highest threshold.

For $p_T > 3.5$ GeV/c, the two photons from over 94% of the π^0 decays were not resolved in the lead glass counters, and a π^0 was defined as a single energy cluster spread over a matrix of at most 3 x 3 adjacent counters. The angle of the π^0 was determined by the centroid of the energy cluster and the interaction vertex. Clusters with their centroids in edge counters were rejected.

The observed π^0 energy was corrected to take into account the response of the lead glass counters, which was measured to be a linear function of the incident angle α. The typical correction was + 9% at α = 0.40 radian. A further correction was applied to account for the energy lost when the decay photons converted in the magnet coil or cryostat. Photon conversion occurred with a probability of $\sim$ 50% and was indicated by the presence of more than 1.5 single ionisation in the B counters facing the energy cluster, after subtracting the contribution of any charged particle tracks observed. The size of the correction varied between + 4% and +5% over the π^0 energy range covered in this experiment.

In addition to high p_T π^0's from beam-beam collisions, the triggers were caused by cosmic rays and particles produced by interactions of the circulating protons with the residual gas or in the walls of the ISR vacuum chamber. For the data at $\sqrt{s}$ = 53.1 and 62.4 GeV, these backgrounds were reduced to a negligible level by the requirements that an interaction vertex with at least two tracks be present, and that 4 or more A counters give signals within ± 15 nsec of the trigger. Since the data at $\sqrt{s}$ = 30.7 GeV were taken with the magnet and drift chambers switched off, only the A counter requirement could be used. In this case some residual background remains in the π^0 sample, whose contribution is at most 5% at the upper end of the p_T range. The efficiencies of the A counter and vertex requirements were measured to be 98% and 90%, respectively, at low values of p_T, where the backgrounds were negligible.

The invariant cross sections in bins of centre-of-mass transverse momentum, p_T, were first obtained separately for the two lead glass arrays, averaged over their centre-of-mass rapidity and azimuthal acceptances, $\Delta y\ \Delta\phi$ = 0.80 and 1.33, respectively. These cross-sections were found to be consistent within the systematic uncertainties, so that the final result was obtained by averaging the two values corresponding to the same p_T bin. This consistency represents a good check that backgrounds have been eliminated, since the backgrounds noted above produce centre-of-mass energy depositions which differ by 30% in the two arrays, resulting in contributions to the cross-sections which differ by a factor of $\sim$ 3.

The invariant cross-sections are shown in Fig. 2 and given in Table II as a function of p_T for the three values of $\sqrt{s}$. The A counter and vertex efficiency corrections have been applied as well as a small correction for smearing due to : individual lead glass block energy resolution

of $\Delta E/E$ (r.m.s.) = 0.004 + 0.043/$\sqrt{E(GeV)}$, as measured for incident electrons; 5% r.m.s. block-to-block calibration variation; and fluctuations in the energy lost by the π^0 in case of photon conversion in the cryostat and coil of the magnet. In addition to the errors shown, there is a systematic uncertainty of $\sim$ 5% in the absolute p_T scale, which is equivalent to $\sim \pm$ 25% uncertainty in the absolute normalization. There is a further uncertainty of $\pm$ 15% in the normalization of the $\sqrt{s}$ = 30.7 GeV data relative to those at 53.1 and 62.4 GeV, because the lowest energy data were taken with no magnetic field. Also, there is a possible error of $\pm$ 5% in the relative normalization at 53.1 and 62.4 GeV, due principally to the luminosity monitoring.

Also shown in Fig. 2 are the data and best fit of a previous experiment, CCRS [6]. For $p_T < 6$ GeV/c, the two experiments are in excellent agreement, except possibly at $\sqrt{s}$ = 53.1 GeV. However, for $p_T > 7$ GeV/c the present data are systematically higher than the extrapolated CCRS fit.

An estimate has been made of the effect of two π^0's overlapping in the same energy cluster, using data on associated charged particles obtained in this experiment [17]. It was found that the contribution to the cross-section from two overlapping π^0's decreased from 6% at p_T = 3 GeV/c to 2% at p_T = 14 GeV/c, and no correction was applied to the data for this effect [18].

The possibility that the events at high p_T might be caused by particles other than π^0's has been investigated by studying the fraction of events without photon conversions as a function of p_T (Fig. 3). The non-conversion fraction is consistent with a constant value of 0.25 over the p_T and $\sqrt{s}$ values covered by the data. This is the value expected for two-photon events. Single photon events [19] would result in a value of 0.5, whereas, for example, 0.06 is expected in the case of events consisting of two π^0's. The data in Fig. 3 are such that a single photon contribution as large as 30% below 10 GeV/c cannot be excluded. Above 10 GeV/c the errors are too large to reach a conclusion on the magnitude of a possible one photon contribution.

It is concluded, therefore, that the results of Fig. 2 are consistent with being all due to two photons. These could be from η-mesons [20] as well as π^0's. However, no correction was applied to the data for an η contribution [21].

In Fig. 4 the invariant cross-section is plotted as a function of x_T for the three values of $\sqrt{s}$. If the data were described by the universal form given by Eq. (1), the curves of $Ed^3\sigma/dp^3$ vs. x_T at two different values of $\sqrt{s}$, $\sqrt{s_1}$ and $\sqrt{s_2}$, would have a constant ratio equal to $(\sqrt{s_2}/\sqrt{s_1})^n$. This is not the case as the ratio of the data at $\sqrt{s}$ = 53.1 and 62.4 is seen to be a function of x_T. These results are summarised in Fig. 5, where n is plotted as obtained at several fixed values of x_T. When using the data at $\sqrt{s}$ = 53.1 and 62.4 GeV, n varies from a value of $\sim$ 8 at low x_T to a value of $\sim$ 5 at high x_T. A larger value of n $\sim$ 6.5 is obtained at high x_T using the data at $\sqrt{s}$ = 30.7 and 53.1 GeV. These results are inconsistent with the scaling law described by Eq. (1), either with constant n or with n a function of x_T.

The same conclusion is obtained by fitting the data at $\sqrt{s}$ = 53.1 and 62.4 GeV within $0.2 < x_T < 0.45$ to Eq. (1) with a specific form $F(x_T) = A(1-x_T)^m$. The best fit values with the present data are n = 6.4 and m = 11.1. These values are similar to a recent experiment of Clark et al. [22]. However, the χ^2 of the fit for the present data is 209 for 34 degrees of freedom, indicating again that Eq. (1) does not provide an adequate description.

It is possible to obtain good fits at the two $\sqrt{s}$ values 53.1 and 62.4 GeV together, by restricting the p_T intervals used. For $3.7 < p_T < 7.0$ GeV/c, with $F(x_T) = A \exp(-bx_T)$, the best fit parameters are n = 8.0 ± 0.4 and b = 6.4 ± 2.5. While n is in good agreement with the value given by CCRS [6], the present value of b is significantly lower [23]. For $7.5 < p_T < 14.0$ GeV/c the best fit parameters of the present data are n = 5.13 ± 0.14 and b = 17.3 ± 0.4. The value of n is found to be constant within errors as the lower limit of the p_T range used in the fit is raised above 7.5 GeV/c. For $F(x_T) = A(1-x_T)^m$ the best fit parameters are n = 8.1 ± 0.4 and m = 5.2 ± 2.1 at low p_T and n = 5.06 ± 0.14 and m = 12.1 ± 0.3 at high p_T.

A possible ± 5% relative normalization error between $\sqrt{s}$ = 53.1 and 62.4 GeV changes the parameter n by ± 0.33 in all cases, and b by ± 1.0. Note that these systematic errors cancel in comparing the values of n obtained at [illegible] and [illegible], [illegible] above, attempts to fit

simultaneously the data at the three $\sqrt{s}$ values using Eq. (1) give unacceptably large χ^2 values.

In conclusion, the present results cannot be described by the simple scaling law of Eq. (1). However, it is still possible to obtain a good fit using only the data at high p_T ($p_T > 7.5$ GeV/c) at the two highest $\sqrt{s}$ values (53.1 and 62.4 GeV). In this case, the exponent n is 5.2 ± 0.4, where the error includes the systematic uncertainties.

Acknowledgements.

We wish to thank J. Bibby, R. Bouhot, H. Cunitz, F. Doughty, R. Gros, R.H. Harfield, G. Kantardjian, J. Renaud, W. Sippach, B. Smith and the P.A. Group, Rutherford Lab, for their invaluable technical help. We are grateful to C. Onions for providing programing help. We acknowledge the excellent performance of the ISR machine. Finally, we thank M.A. Huber for help with data handling.

Table I

Integrated Luminosities (cm^{-2})

Nominal p_T at threshold (GeV/c)	$\sqrt{s}$ (GeV) 30.7	53.1	62.4
3.0	-	1.20×10^{34}	2.38×10^{34}
3.5	1.39×10^{36}	-	-
5.0	-	-	5.60×10^{35}
7.0	-	1.41×10^{37}	1.58×10^{37}

Table II

Invariant Cross Sections for the Reaction

$p + p \rightarrow \pi^0 + \text{anything}$

$\sqrt{s}$ (GeV)	p_T (GeV/c)	$E\frac{d^3\sigma}{dp^3}$ (cm^2c^3/GeV^2)	$\sqrt{s}$ (GeV)	p_T (GeV/c)	$E\frac{d^3\sigma}{dp^3}$ (cm^2c^3/GeV^2)
30.7	4.19	$(1.69\pm0.02) \times 10^{-33}$	62.4	3.72	$(3.92\pm0.31) \times 10^{-32}$
	4.70	$(4.88\pm0.09) \times 10^{-34}$		4.22	$(1.26\pm0.09$
	5.19	(1.46 ± 0.04)		4.72	$(4.16\pm0.50) \times 10^{-33}$
	5.69	$(4.70\pm0.28) \times 10^{-35}$		5.22	(1.79 ± 0.15)
	6.19	(1.82 ± 0.13)		5.72	$(8.00\pm0.62) \times 10^{-34}$
	6.68	$(8.4 \pm1.1) \times 10^{-36}$		6.21	(4.00 ± 0.36)
				6.71	(1.83 ± 0.14)
53.1	3.71	$(3.52\pm0.29) \times 10^{-32}$		7.20	$(9.17\pm0.78) \times 10^{-35}$
	4.21	(1.08 ± 0.14)		7.70	(4.44 ± 0.08)
	4.71	$(3.83\pm0.50) \times 10^{-33}$		8.21	(2.44 ± 0.07)
	5.21	(1.48 ± 0.21)		8.71	(1.43 ± 0.03)
	5.71	$(6.5 \pm1.1) \times 10^{-34}$		9.21	$(7.92\pm0.24) \times 10^{-36}$
	7.70	$(2.09\pm0.05) \times 10^{-35}$		9.70	(4.56 ± 0.29)
	8.20	(1.14 ± 0.05)		10.20	(2.55 ± 0.13)
	8.70	$(6.10\pm0.27) \times 10^{-36}$		10.70	(1.36 ± 0.11)
	9.20	(3.18 ± 0.17)		11.20	$(8.83\pm0.75) \times 10^{-37}$
	9.70	(1.78 ± 0.13)		11.70	(5.20 ± 0.55)
	10.19	$(9.85\pm0.87) \times 10^{-37}$		12.20	(3.76 ± 0.55)
	10.69	(6.50 ± 0.96)		12.70	(2.07 ± 0.47)
	11.19	(4.05 ± 1.05)		13.19	(1.80 ± 0.31)
	11.69	(1.75 ± 0.60)		13.68	$(9.2 \pm2.2) \times 10^{-38}$
	12.19	(1.29 ± 0.34)			
	12.69	$(6.5 \pm2.6) \times 10^{-38}$			

REFERENCES

1) F.W. Büsser et al., in Proc. of the 16th International Conference on High Energy Physics, Batavia, Illinois (1972). Vol. 3, p. 317.

2) B. Alper, et al., Phys. Letters 44B (1973) 521.

3) M. Banner, et al., Phys. Letters 44B (1973) 537.

4) F.W. Büsser, et al., Phys. Letters 46B (1973) 471.

5) K. Eggert, et al., Nuclear Phys. B98 (1975) 49.

6) F.W. Büsser, et al., Nuclear Phys. B106 (1976) 1.

7) J.W. Cronin, et al., Phys. Rev. D11 (1975) 3105.

8) G. Donaldson, et al., Phys. Rev. Letters 36 (1976) 1110.

9) D. Antreasyan, et al., Phys. Rev. Lett. 38 (1977) 112.

10) S.M. Berman, et al., Phys. Rev. D4 (1971) 3388.

11) R. Blankenbecler, et al., Phys. Rev. D12 (1975) 3649.

12) R.D. Field, Phys. Rev. Lett. 40 (1978) 997.

13) M. Morpurgo, Cryogenics 17 (1977) 89.

14) L. Camilleri, et al., in Proc. of the Wire Chamber Conference, Vienna (Austria) (1978). (To be published in Nucl. Instrum. Methods).

15) J. S. Beale, et al., Nucl. Instrum. Methods 117 (1974) 501.

16) S. Van der Meer, CERN Internal Report ISR-PO/68-31 (1968).

17) A.L.S. Angelis, et al., Results on Correlations and Jets in High Transverse Momentum p-p Collisions at the CERN ISR, submitted to the XIX International Conference on High Energy Physics, Tokyo, August 1978.

18) The decrease of this effect with increasing p_T is a consequence of the fact that the p_T distribution of particles produced along the direction of a high p_T π^0 was found to be independent of $p_T(\pi^0)$ for $p_T(\pi^0) > 2.5$ GeV/c [17]. Scaling of this distribution with $p_T(\pi^0)$ would have resulted in a magnitude of the overlap correction increasing with p_T from $\sim$ 7% at 3 GeV/c to $\sim$ 10% at 14 GeV/c.

19) G.R. Farrar and J.C. Frautschi, Phys. Rev. Lett. 36 (1976) 1017;
C.O. Escobar, Nuclear Phys. B98 (1975) 174;
E.L. Feinberg, Nuovo Cimento 34A (1976) 391;
F. Halzen and D. Scott, Phys. Rev. Lett. 40 (1978) 1117.

20) F.W. Büsser, et al., Phys. Letters 55B (1975) 232.

21) For instance, if $\eta/\pi = 0.55$, as measured at lower values of p_T (ref. 19), the correction would be $\sim$ - 17%.

22) A.G. Clark, et al., Phys. Letters 74B (1978) 267.

23) However, if the CCRS data at $\sqrt{s}$ = 52.7 and 62.4 GeV are refit with the cut $p_T > 3.7$ GeV/c, their value of b becomes $b = 9.6 \pm 1.3$, in reasonable agreement.

Figure captions

Fig. 1 : A view of the apparatus normal to the solenoid axis.

Fig. 2 : Invariant cross-sections ($cm^2\ c^3/GeV^2$) for the reaction $p + p \to \pi^0$ + anything versus p_T. Also shown are the data points from ref. 6 with their best fit using Eq. (1) (dashed lines). The cross-section scale corresponds to the data at $\sqrt{s}$ = 62.4 GeV. For $\sqrt{s}$ = 53.1, the data have been divided by a factor of 10; for $\sqrt{s}$ = 30.6, by a factor of 100.

Fig. 3 : Fraction of events without photon conversion vs.p_T.

Fig. 4 : Invariant cross-section for the reaction $p + p \to \pi^0$ + anything vs. $x_T = 2p_T/\sqrt{s}$.

Fig. 5 : The exponent n of Eq. (1) plotted as a function of x_T, as obtained from Fig. 4, using the two lowest and two highest $\sqrt{s}$ values. The systematic normalization error at $\sqrt{s}$ = 30.6 discussed in the text has been added in quadrature.

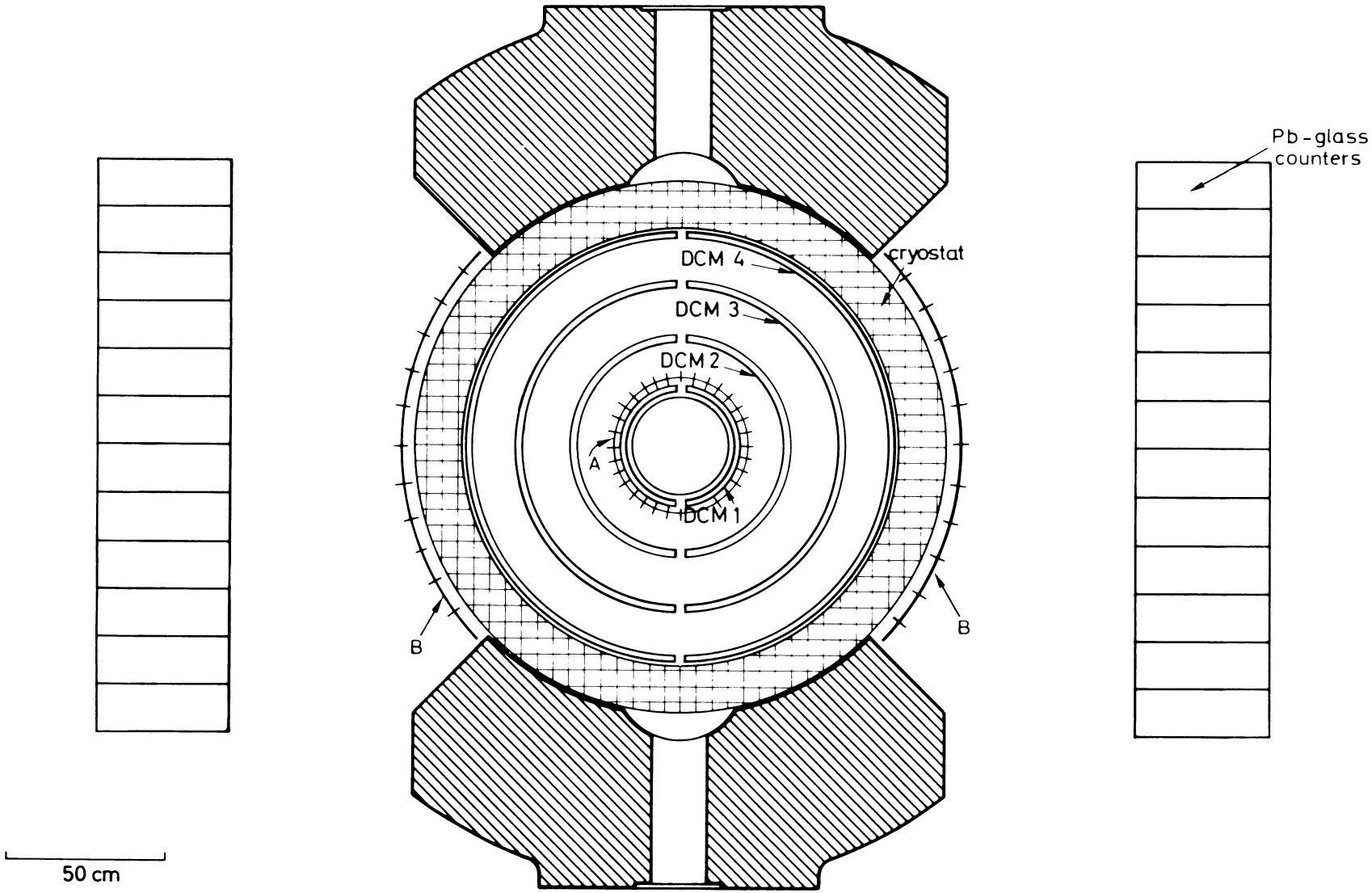

Fig. 1

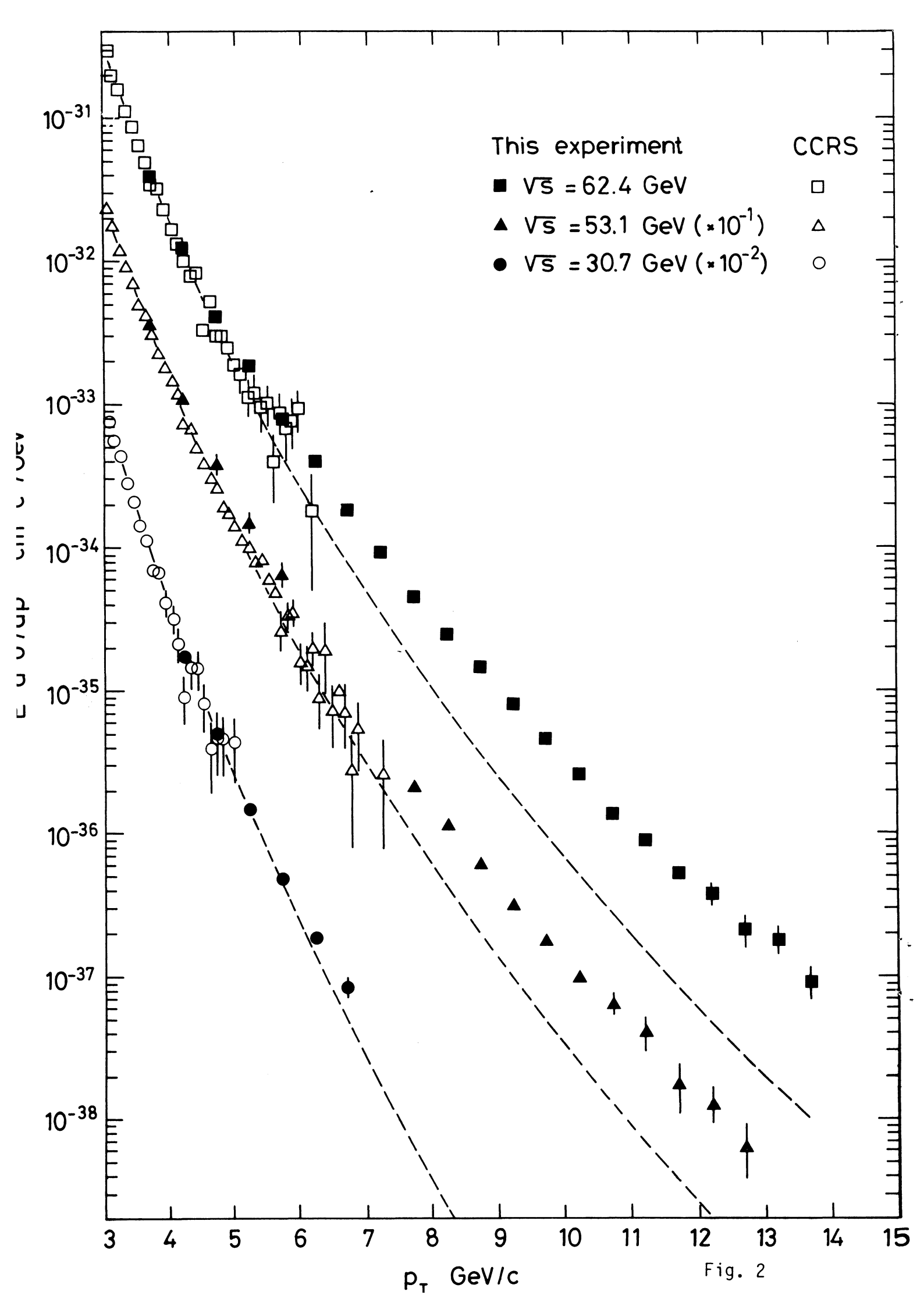
This experiment
CCRS
$\sqrt{s}$ = 62.4 GeV
$\sqrt{s}$ = 53.1 GeV (×10^{-1})
$\sqrt{s}$ = 30.7 GeV (×10^{-2})
10^{-31}
10^{-32}
10^{-33}
10^{-34}
10^{-35}
10^{-36}
10^{-37}
10^{-38}
3
4
5
6
7
8
9
10
11
12
13
14
15
p_T GeV/c

Fig. 2

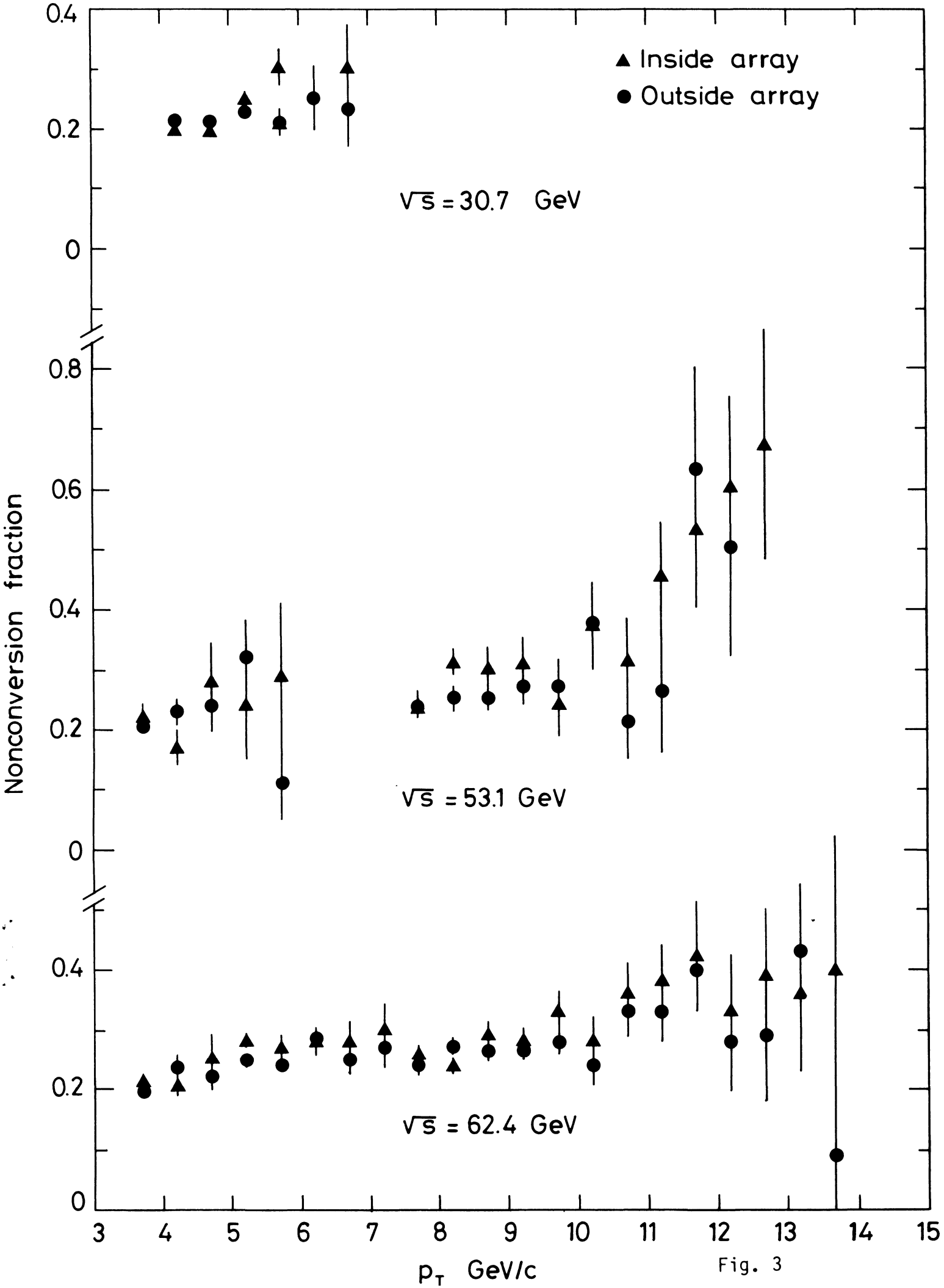
▲ Inside array
● Outside array
√s = 30.7 GeV
√s = 53.1 GeV
√s = 62.4 GeV
Nonconversion fraction
p_T GeV/c
0.4
0.2
0
0.8
0.6
0.4
0.2
0
0.4
0.2
0
3
4
5
6
7
8
9
10
11
12
13
14
15

Fig. 3

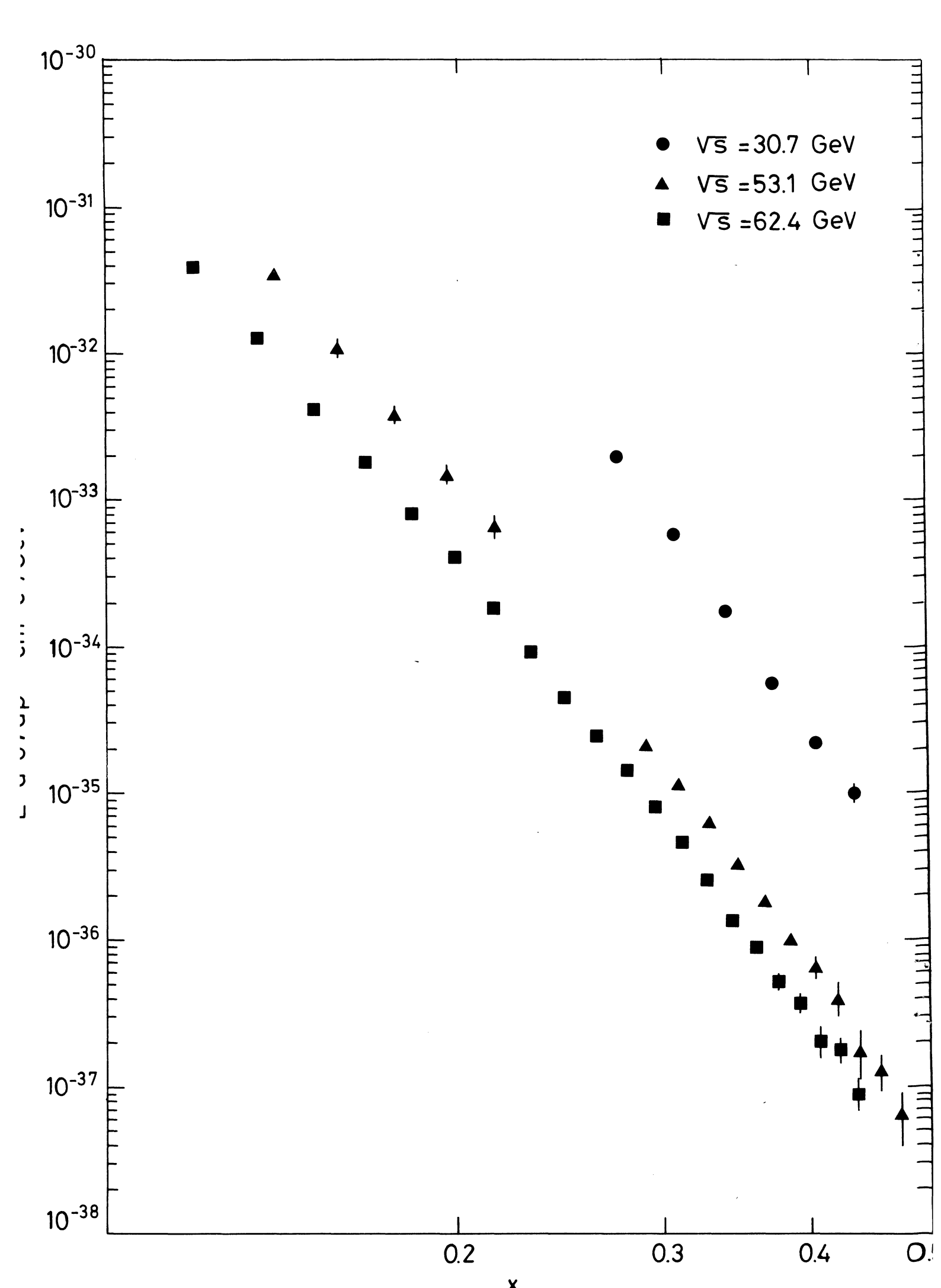
10^{-30}
10^{-31}
10^{-32}
10^{-33}
10^{-34}
10^{-35}
10^{-36}
10^{-37}
10^{-38}
$\sqrt{s}$ =30.7 GeV
$\sqrt{s}$ =53.1 GeV
$\sqrt{s}$ =62.4 GeV
0.2
0.3
0.4
x_T

Fig. 4

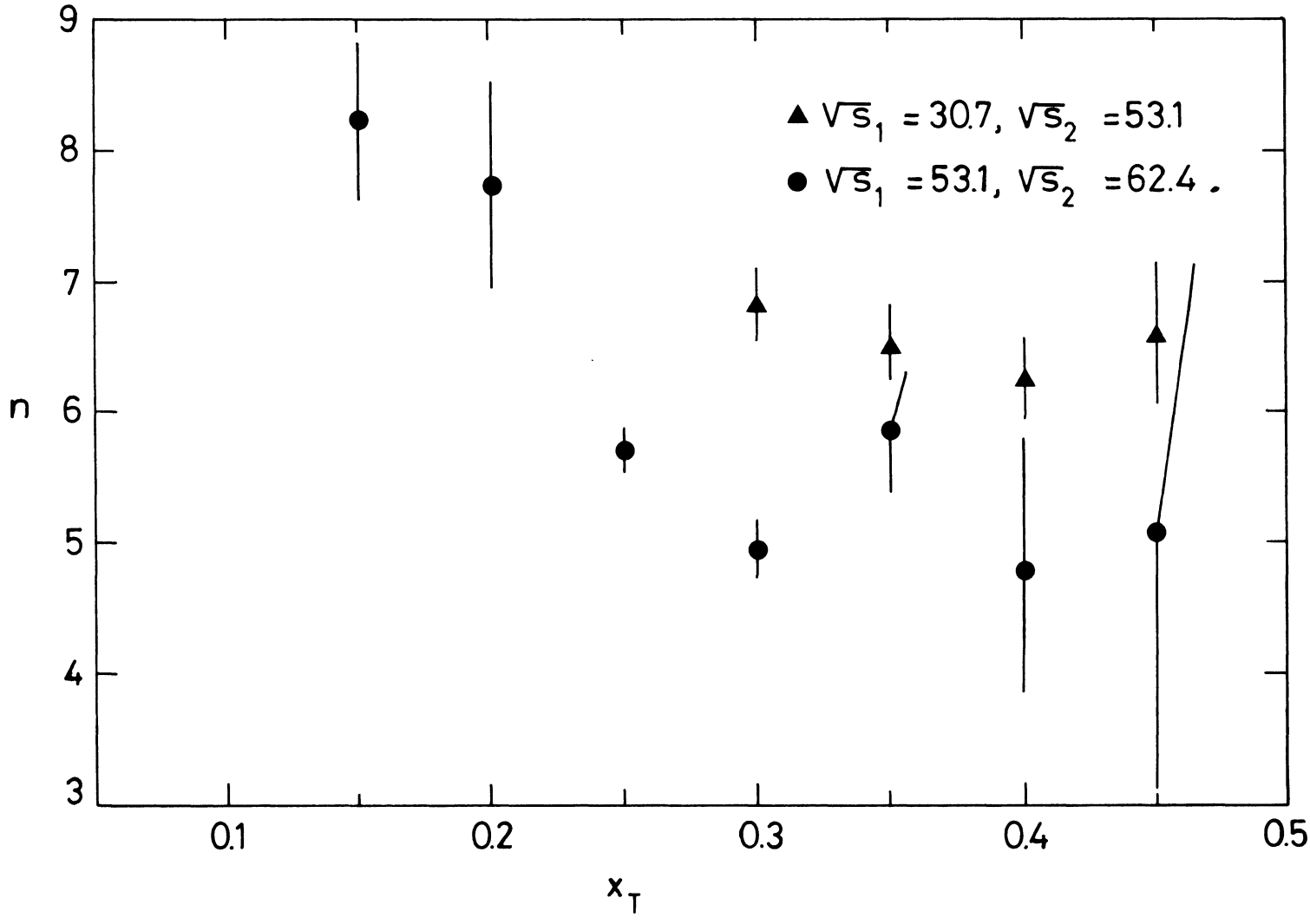
9
8
7
6
5
4
3
n
0.1
0.2
0.3
0.4
0.5
x_T
▲ $\sqrt{s}_1 = 30.7$, $\sqrt{s}_2 = 53.1$
● $\sqrt{s}_1 = 53.1$, $\sqrt{s}_2 = 62.4$

Fig. 5

APPENDIX III

RESULTS ON CORRELATIONS AND JETS IN HIGH TRANSVERSE MOMENTUM p-p COLLISIONS AT THE CERN ISR

CERN[1]-Columbia[2]-Oxford[3]-Rockefeller[4] (CCOR) Collaboration

A.L.S. Angelis[3], B.J. Blumenfeld[2], L. Camilleri[1], T.J. Chapin[4], R.L. Cool[4], C. del Papa[1], L. Di Lella[1], Z. Dimčovski[4], R.J. Hollebeek[2], D. Levinthal[2], L.M. Lederman[2], J.T. Linnemann[4], L. Lyons[3], N. Phinney[3], B.G. Pope[1*)], S.H. Pordes[1], A.F. Rothenberg[4**)], A.M. Segar[3], J. Singh-Sidhu[1], A.M. Smith[1], M.J. Tannenbaum[4], R.A. Vidal[2***)], J. Wallace-Hadrill[3], T.O. White[3†)] and J.M. Yelton[3]

ABSTRACT

A large solid-angle apparatus consisting of a superconducting solenoid magnet, cylindrical drift chambers, and two arrays of lead-glass counters is used to examine particles associated with a high transverse momentum trigger in pp interactions at the CERN ISR.

The trigger is given by energy deposition in the lead-glass arrays centred at 90°. Results on particle correlations and on jets are presented for interactions at $\sqrt{s}$ = 62.4 GeV and in the trigger transverse momentum range $3 < p_T < 11$ GeV/c.

Submitted to the
XIX International Conference on High Energy Physics
Tokyo, August 1978

Geneva - 29 September 1978

---

*) Present address: Physics Dept., Princeton University, NJ, USA.
**) Present address: CERN, Geneva, Switzerland.
***) Present address: Stanford Linear Acc. Center, Stanford, CA, USA.
†) Present address: Cavendish Laboratory, University of Cambridge, U.K.

1. Introduction

The observation of unexpectedly high hadron-hadron inclusive production at large transverse momentum several years ago [1] has led to considerable experimental and theoretical effort to understand these phenomena. Some of the principal sources of data are the experiments that investigate the correlations between the particles produced in such a high transverse momentum collision. This paper reports the preliminary results obtained by the CCOR Collaboration at the CERN Intersecting Storage Rings (ISR).

Previous correlation studies [2] at the CERN ISR have helped the development of a jet theory of high-p_T interactions. Each experiment has improved on its predecessors by adding momentum measurement, improving the solid angle, or raising the trigger energy. Momentum measurement is necessary to investigate resonance structure and to study the correlation effects as a function of the momentum of particles. A large solid angle is needed to contain the event in the apparatus and to demonstrate that the effects observed are independent of the acceptance cut of the apparatus. A high trigger energy is desirable because the strength of the correlations (the jet-like nature of the events) is expected to increase with the trigger transverse momentum. Unfortunately, no single experiment has succeeded in doing all three. In particular, no apparatus has had momentum measurement over the full azimuth. The experiment discussed in this paper goes further by combining a high-p_T lead-glass trigger covering $\sim$ 2 sr, with charged particle momentum measurement over the full azimuth and a limited rapidity

interval. The lead-glass trigger system together with the improved luminosity of the ISR now allows study of triggers with $p_T \sim 10$ GeV/c, as compared to previous experiments with $p_T \sim 4$ GeV/c.

2. Apparatus

The apparatus (Fig. 1) consists of a 1.5 tesla aluminium-stabilized superconducting solenoid which contains cylindrical drift chambers surrounding the interaction region. In addition, there are two walls of lead-glass total absorption Čerenkov counters, each covering a solid angle of ~ 1 sr.

The solenoid has a usable cylindrical volume 170 cm long with a radius of 70 cm. Its field of 1.5 tesla is uniform to 1.5% over the entire solid angle covered by the four cylindrical drift-chamber modules (DCM1-DCM4). Each module contains two layers of drift chambers. They are of the adjustable electric field design to allow for compensation of magnetic field forces over drift distances up to 2.2 cm. The 580 sense wires of this system are parallel to the magnetic field, and the drift time is used to measure the ϕ coordinates of charged tracks passing through the chambers. This is the coordinate that requires the most accuracy, as it determines the transverse momentum p_T of the tracks. The left-right sense wire ambiguity in each module is partially resolved by the angular offset of the outer gap's sense wires with respect to those of the inner by half the sense-sense angle. Delay lines are glued to one of the cathode planes facing each of the 580 sense wires. An avalanche on the sense wire induces a pulse on the delay line. The z coordinate (along the solenoid axis) can then be extracted from the

times of arrival of this induced pulse at the two ends of the delay line. Thus, by providing pairs of ϕ and z coordinates, the system reduces the off-line computing load by eliminating the need for ϕ and z matching. In addition, the solenoid contains a barrel hodoscope of 32 counters ("A") between DCM1 and DCM2 which are used to give a timing signal for each event and to check the validity of tracks. More information on the solenoid [3] and the chambers [4] can be found elsewhere.

The detector is triggered by energy deposition in either of the two walls of lead glass [5] located just outside the thin-walled ($\sim$ 1 r.l.) region of the solenoid at a distance of 140 cm from the intersection region. Each wall consists of 168 blocks arranged into a 12 × 14 array. The blocks are 15 × 15 × 40 cm (17 r.l.). They are calibrated using a monoenergetic electron beam at the CERN Proton Synchrotron (PS). This calibration is monitored by recording the pulse height of the light emitted by small NaI crystals, doped with ^{241}Am, which are glued to each block. Further checks on the calibration are provided by monitoring the magnitude of the pulse-height peak produced by charged hadrons traversing an entire block and by measuring the π^0 mass in events containing two well-separated photons. Both of these checks are made with the glass withdrawn to 350 cm from the intersection region. Two 12-counter hodoscopes ("B") located between the magnet and the glass are used to sense the showering of particles in the solenoid coil and to allow correction for the energy loss due to this effect.

3. Analysis and cuts

Data have been taken with the ISR operating at $\sqrt{s}$ = 62.4 and at luminosities up to 4×10^{31} cm^{-2} s^{-1}. They can be divided into four groups with different centre-of-mass trigger thresholds: i) zero -- the trigger is provided by a pulse from any one of the A counters; ii) $p_T > 3$ GeV/c; iii) $p_T > 5$ GeV/c; and, iv) $11 > p_T > 7$ GeV/c.

Tracks are reconstructed (≥ 5 points) and vertices are found for all events. Events whose tracks do not form a vertex in the "diamond" intersection region of the two beams are rejected. High p_T events with less than four A-counters are rejected to reduce background at very high p_T. Tracks are discarded if they do not point to the vertex or if they do not have A-counter signals in time (±15 ns) with the event. The track reconstruction efficiency is $\sim$ 80%; the vertex cut removes 10% of the good events from the sample. The r.m.s. momentum resolution is

$$\Delta p_T/p_T \sim \sqrt{(0.02)^2 + (0.07\ p_T)^2} \qquad (p_T \text{ in GeV/c}) ,$$

where the first term is due to multiple coulomb scattering and the second results from a $\sim$ 500 μ drift-chamber resolution. The track reconstruction losses are predominantly due to drift chamber inefficiency. The inefficiency of the vertex cut is due to track losses and to the extrapolation errors due to drift chamber resolution. The momentum resolution is for a long running-period early in the operation of the system, and includes effects of uncertainties in the chamber alignment as well as in the time-distance relations in the chambers. It is also influenced by the ϕ ambiguities

occurring when only one point out of the two in a module is present, and by the shorter lever arm available for tracks which lose both points in DCM1 or DCM4.

The energy deposited in the glass is required to come from clusters not larger than 3 × 3 blocks. It is corrected for the angle between the incoming photon(s) and the glass, and for the energy loss in the solenoid wall using information from the associated B counters. The r.m.s. energy resolution of the lead glass is $\Delta E/E \sim 0.05 + + 0.04/\sqrt{E}$. There is a systematic uncertainty of $\sim$ 5% in the absolute energy calibration of the lead glass.

The laboratory momenta of all particles are transformed to the centre-of-mass system assuming that the particles are pions. Pseudo-rapidities $\{\eta = -\ln [\tan (\theta/2)]\}$ are calculated for each particle. The trigger particle is defined to be the neutral particle with the maximum p_T. This p_T is required to be above the threshold cut for the data set. Events in which a charged particle strikes the glass within 28 cm of the trigger cluster are rejected. This cut eliminates clusters whose energy is partly from a charged particle. It also rejects high-momentum electrons from Dalitz decay or conversion of neutrals in the vacuum pipe and chambers which would otherwise be considered as associated hadrons. This cut biases the study of correlations on the same side as the trigger. The correlations on the side opposite to the trigger are not affected by such a cut. Acceptance cuts are applied so as to make the apparatus symmetric in the centre-of-mass system. The cuts used for the trigger particle and the associated particles are given in Table I. Table II contains the number of events and tracks passing these cuts.

For this preliminary analysis, no corrections have been made for efficiency or momentum and energy resolution.

4. Charged particle correlations

One of the simplest correlations is the azimuthal correlation of charged tracks with the trigger particle. These are shown in $dn/d\phi$ plots (Fig. 2) for five 1 GeV/c bands of charged particle transverse momentum, where $dn/d\phi$ is the average number of tracks per unit azimuth per event with trigger $p_{T\,t} > 7$ GeV/c. The azimuth of a track is measured relative to that of the trigger. The plot is split into two halves for the same ($|\phi| < \pi/2$, Fig. 2a) and away ($|\phi - \pi| < \pi/2$, Fig. 2b) sides. Strong correlation peaks on top of flat backgrounds can be seen in all plots. In each band the level of the flat background is similar to that found in the zero threshold trigger. The same-side correlation peaks shown here have been diminished from their true values, and their shapes have been changed because of the cut on track-to-cluster distance explained in the previous section. The width of the away-side peak shrinks with increasing charged particle p_T, as is expected in almost all models. This will be discussed later using the variable p_{out}. The FWHM $\sim$ 1 radian at low p_T shows that the correlation enhancement extends over almost all of the away side. The away-side azimuthal correlation for all tracks with $p_T > 0.3$ GeV/c is shown for four 1 GeV/c bands of trigger $p_{T\,t}$ (Fig. 3). The peak becomes higher and narrower as the trigger $p_{T\,t}$ increases.

Another possible correlation is that between the rapidity of the away-side charged particle and the trigger. Historically no effect

has been seen. This remains true in this experiment as shown in the plots of $dn/d(\eta_{track} - \eta_{trigger})$ (Fig. 4a). The triangular shape observed is that expected from the folding together of two independent flat η distributions ($|\eta| < 0.5$ for the trigger and $|\eta| < 0.7$ for charged particles). A plot of $dn/d(\eta_{track} + \eta_{trigger})$ has the same shape. A rapidity correlation can be observed between charged particles on the away side and the maximum p_T particle on the away side (leader). This was one of the earliest observed effects which supported a "jet" picture of high p_T interactions. It is shown in the $dn/d(\eta_{track} - \eta_{leader})$ plot (Fig. 4b). This correlation is also observed to shrink in width as a function of the p_T track.

The information from all four data sets can be compared by studying the variation with track p_T and trigger $p_{T\,t}$ of the following correlation functions defined for the away side and calculated using $dn/d\phi$ distribution of the type shown in Fig. 2b:

$$\bar{f}(p_T,\ p_{T\,t}) = \frac{\Delta n}{\Delta p_T\ \Delta\eta\ \Delta\phi}(p_T,\ p_{T\,t}) = \frac{1}{\Delta p_T\ 1.4\ \pi}\int_{\pi/2}^{3\pi/2} d\phi\ \frac{dn}{d\phi}(\phi)\ ,$$

$$f_{max}\ (p_T,\ p_{T\,t}) = \frac{1}{\Delta p_T\ 1.4}\frac{dn}{d\phi}(\phi = \pi), \quad \Delta p_T = 1.0\ \text{GeV/c}\ .$$

They are shown in Figs. 5a and 5b, respectively; $\bar{f}(p_T,\ p_{T\,t})$ shows how the number of charged particles averaged over the entire away side varies as a function of their p_T for trigger transverse momentum above $p_{T\,t}$, while $f_{max}(p_T,\ p_{T\,t})$ shows the changes in the peak number of particles. Previous experiments with small azimuthal acceptance could only measure f_{max}. The strong correlation increasing with

p_T and $p_{T\,t}$ has been seen before but not for such a wide range of $p_{T\,t}$. The average multiplicity $\bar{F}(p_{T\,t})$ of tracks ($p_T > 0.3$ GeV/c) per unit rapidity and unit azimuth on the away side is derived from the $dn/d\phi$ distributions of Fig. 3 and is plotted in Fig. 5c. Figure 5d shows the multiplicity $F_{max}(p_{T\,t})$ of tracks ($p_T > 0.3$ GeV/c), per unit rapidity and unit azimuth at $\phi = \pi$, which is the maximum of the correlation on the away side. The plot of $\bar{F}$ shows that the multiplicity is rising as a function of $p_{T\,t}$. The fact that F_{max} rises faster than $\bar{F}$ shows that the azimuthal peak must be shrinking as a function of $p_{T\,t}$.

It has become standard practice to study dn/dx_E and $\langle|p_{out}|\rangle$ distributions as a function of x_E. These variables are defined in Fig. 6. The results for $\langle|p_{out}|\rangle$ (Fig. 7a) do not appear to scale in x_E for different $p_{T\,t}$. Agreement with previous results [6] is reasonable for the low threshold data. It can also be seen that at constant p_T (Fig. 7b), $\langle|p_{out}|\rangle$ is higher for low $p_{T\,t}$. It should be noted that these plots have not been corrected for the effects due to momentum resolution.

In parton models p_{out} is often thought of as being composed of two contributions, one from the transverse momentum of the two partons that enter the hard scattering process k_T, and the other from the transverse momentum given to a particle during the fragmentation of its parent parton after the scattering q_T. In this picture

$$\langle|p_{out}|\rangle = \sqrt{\langle k_T\rangle^2\, x_E^2 + \frac{1}{2}\langle q_T\rangle^2\,(1 + x_E^2)}\ .$$

One of the striking features of previous experiments [6] was the increase of $\langle |p_{out}| \rangle$ with x_E, which led to the introduction of models in which $\langle k_T \rangle$ was forced to be much greater than the originally expected value of $\langle k_T \rangle \sim 0.3$ GeV/c. In order to explain the p_T imbalance in high-mass electron pair production at FNAL [7], a value of $\langle k_T \rangle \sim 0.85$ GeV/c has been used [8]. The results shown in Fig. 7 suggest an even larger value of $\langle k_T \rangle$ and also a dependence of $\langle k_T \rangle$ on the trigger $p_{T\,t}$.

The dn/dx_E spectra (Fig. 8) appear to scale in x_E. However, it is important to remember that these distributions have not been corrected for momentum resolution. To study these correlations further, the azimuthal acceptance is restricted to a region $|\phi - \pi| < \pi/3$. As can be seen from the azimuthal distributions (Fig. 2), such a cut contains the correlated peak. A distribution of the total charged x_E, the sum of the x_E's of all of the charged tracks, for three 1 GeV/c intervals of trigger $p_{T\,t}$ is shown in Fig. 9. No cuts are made on the direction or magnitude of the sum of the momenta. Thus the plot shows the distribution of balancing momentum that falls in a fixed rapidity interval independent of the direction of the away-side jet. The x_E scaling of this distribution is fairly good in the interval considered, but again no corrections are made for momentum resolution.

Same-side charged particle correlations with the trigger are also studied in a restricted ϕ region ($|\phi| < \pi/3$) which contains the correlation peak. In order to be able to use more of the same-side correlated charged particles, tracks pointing to within 20 cm of the trigger energy in the lead glass are excluded, but the event

is still used. This cut excludes a $\sim$ 0.05 sr disk around the trigger in the centre-of-mass system. The trigger neutral is required to have $|\eta| < 0.4$ to ensure a large solid angle for tracks accompanying it. The single-particle transverse momentum distribution (Fig. 10) is found to be almost independent of the trigger $p_{T\,t}$ for all three sets of data. Summing the x_E of all charged tracks in the same-side region and averaging over all events gives the mean values of the total charged x_E as a function of trigger $p_{T\,t}$ (Fig. 11). The accompanying momentum on the same side is a small fraction of $p_{T\,t}$. This is a demonstration of the trigger bias introduced by a neutral cluster trigger requirement.

In the two remaining 60° regions, $\pi/3 < |\phi| < 2\pi/3$, which are outside the correlation enhancements, the shape of the single-particle momentum spectrum can be seen to differ only slightly from the zero threshold spectrum (Fig. 12).

5. Correlations to a vector sum

The correlations between away-side particles provide an important test of the constituent hard-scattering model of high p_T particle production. The constituent should fragment into particles whose momenta are distributed symmetrically about the constituent's momentum vector. In this analysis, the vector sum of the observed charged particles' momenta is used to approximate this vector. Missing neutral and undetected charged particles can affect the direction and magnitude of the measured total momentum, hence the results are only suggestive and not quantitative.

The vector sum is constructed from the charged particles on the away side with $|\phi-\pi| \leq \pi/3$ and $|\eta| < 0.7$. Events are selected which have $|\eta_{sum}| < 0.3$ and $p_{T\,sum} > 3$ GeV/c. The first cut ensures that events are centred in the apparatus. The second cut eliminates events containing only low-energy spectator hadrons. Only data with $p_{T\,t} > 7$ GeV/c are used.

The fragmentation about the axis is defined in terms of two variables $|p_{out\,\phi}|$ and $|p_{out\,\theta}|$ (Fig. 13). The mean values for these quantities are plotted in Fig. 14 as a function of the p_T of the particle. They are approximately equal and limited to about 0.35 GeV/c. The dip at 3 GeV is due to the threshold for events with only one away-side particle which satisfies the cuts and gives $p_{out} = 0$.

The data can be compared with curves generated by a Monte Carlo simulation, which are shown on the same plots. For the simulation, a trigger p_T is picked from the observed distribution. An away-side multiplicity is chosen according to the distribution of multiplicities seen for centred events ($\langle n_{ch} \rangle = 3.5$). Charged particle momenta are selected from the measured p_T distribution associated with the chosen trigger p_T. For $p_{out\,\theta}$, the θ of the track is picked from a flat distribution since no θ correlation is observed. In $p_{out\,\phi}$, there are two curves: in the upper curve ϕ is picked according to a flat distribution; in the lower curve ϕ is picked according to the five $dn/d\phi$ plots of Fig. 2.

The $\langle |p_{out\,\phi}| \rangle$ and $\langle |p_{out\,\theta}| \rangle$ from the Monte Carlo simulation rise to values of 0.9 and 0.75 GeV/c, respectively. The difference between these values and the data demonstrates that the maximum

values seen in the data are not due to the limitations of the acceptance used in this analysis. Inclusion of the ϕ correlations lowers the $\langle |p_{out\,\phi}| \rangle$ to 0.55 GeV/c, which is still significantly higher than the data. The fact that the Monte Carlo curves also level off (though at a higher-track p_T) reflects the degree to which a single high-momentum particle dominates the vector sum. This occurs because the multiplicities are low, and the other particles contributing to the sum have a steeply falling momentum spectrum. The fact that the observed p_{out} values are smaller than those formed with the Monte Carlo simulation indicates that the correlation between away-side particles is stronger than that indicated by their independent correlations to the trigger.

6. Conclusions

The following conclusions can be made from the preliminary results shown for the charged particles produced in association with a high-p_T neutral in p-p collisions at $\sqrt{s}$ = 62.4.

i) The azimuthal correlation of charged particles with a triggering neutral forms two broad peaks at $\phi = 0$ and $\phi = \pi$.

ii) There is no rapidity correlation of away-side charged particles with a neutral trigger, even at the highest trigger p_T.

iii) There is a rapidity correlation of away-side particles relative to the highest p_T particle on the away side.

iv) The width of the away-side azimuthal correlation enhancement decreases with charged particle p_T.

v) The strength of the away-side azimuthal enhancement increases with trigger p_T.

vi) $\langle |p_{out}| \rangle$ increases as a function of x_E and trigger p_T (for fixed x_E) reaching values above 1 GeV/c. (Note: no correction for momentum resolution has been made.)

vii) dn/dx_E appears to scale in x_E over a wide range of trigger p_T. (Note: no correction for momentum resolution has been made.) The same is true for $dN/d(\Sigma x_E)$.

viii) The hadrons in the same-side correlation enhancement have a momentum spectrum which appears to be independent of trigger p_T. The fraction of the energy in charged hadrons accompanying the trigger decreases with trigger p_T.

ix) The shape of the spectrum of tracks outside of the two azimuthal correlation enhancements is the same as that for zero threshold triggers.

x) Reconstructing an away-side jet using only the observed charged particles shows fragmentation that is symmetric about the jet axis.

REFERENCES

1. Alper, B. et al., Phys. Letters 44B, 521 (1973).
Banner, M. et al., Phys. Letters 44B, 537 (1973).
Büsser, F.W. et al., Phys. Letters 46B, 471 (1973).

2. Finocchiaro, G. et al., Phys. Letters 50B, 396 (1974).
Büsser, F.W. et al., Phys. Letters 51B, 310 (1974).
Eggert, K. et al., Nuclear Phys. B98, 73 (1975).
Büsser, F.W. et al., Nuclear Phys. B106, 1 (1976).
Darriulat, P. et al., Nuclear Phys. B107, 429 (1976).
Della Negra, M. et al., Nuclear Phys. B127, 1 (1977).
Albrow, M. et al., Nuclear Phys. B135, 461 (1978).
Bøggild, H., Proc. 8th Symposium on Multiparticle Dynamics, Kaysersberg, France, 1977 (Centre de Recherches nucléaires, Strasbourg, 1977), p. B-1.

3. Morpurgo, M., Cryogenics 17, 89 (1977).

4. Camilleri, L. et al., A system of cylindrical drift chambers in a superconducting solenoid, Paper presented at the Wire Chamber Conference, Vienna, 1978, to be published in Nuclear Instrum. Methods.

5. Beale, J.S. et al., Nuclear Instrum. Methods 117, 50 (1974).

6. Della Negra, M. et al., Nuclear Phys. B127, 1 (1977).

7. Herb, S.W. et al., Phys. Rev. Letters 39, 252 (1977).
Innes, W.R. et al., Phys. Rev. Letters 39, 1246 (1977).

8. Feynman, R.P. et al., CALT-68-651 (1978).

Table I

Acceptance cuts for particles

	p_T	Pseudo-rapidity	Azimuth
Charged	$p_T > 0.3$	$\|\eta\| < 0.7$	No cut
Neutral cluster	$p_T >$ threshold	$\|\eta\| < 0.5$	$\|\phi\| < 0.47$ $\|\phi-\pi\| < 0.47$

Table II

Data Group

Centre-of-mass p_T threshold	None	3 GeV/c	5 GeV/c	7 GeV/c
Average trigger p_T		3.76 GeV/c	5.8	8.0
Luminosity	10^{30}	2.4×10^{34} cm^{-2}	5.6×10^{35}	1.6×10^{37}
No. of events	19,499	10,000	6,600	13,100
Tracks/event	3.2 ± 0.02	6.39 ± 0.02	6.58 ± 0.02	6.74 ± 0.02
$\frac{\text{Tracks}}{\text{Event}}$ (same side) in acceptance region	0.77 ± 0.006	1.15 ± 0.01	1.18 ± 0.01	1.16 ± 0.01
$\frac{\text{Tracks}}{\text{Event}}$ (away side) in acceptance region	0.77 ± 0.006	1.85 ± 0.01	2.23 ± 0.02	2.52 ± 0.01

Figure captions

Fig. 1 : a) A view of the apparatus normal to the solenoid axis. The lead-glass walls were 140 cm from the centre of the solenoid for the data discussed in this paper.

b) Top view of the apparatus.

Fig. 2 : Charged particle correlations.

a) Same-side azimuthal correlation of charged particles relative to the triggering neutral.

b) Away-side azimuthal correlation of charged particles relative to the triggering neutral.

Five plots corresponding to 1 GeV/c intervals in p_T of the charged particle are shown. The data is for trigger $p_T > 7$ GeV/c.

Fig. 3 : Away-side azimuthal correlation of charged particles with $p_T > 0.3$ GeV/c relative to the triggering neutral. Four plots corresponding to 1 GeV/c intervals in $p_{T\,t}$ of the trigger are shown.

Fig. 4 : a) Rapidity correlation of away-side charged particles relative to the triggering neutral.

b) Rapidity correlations of charged particles in the away-side relative to the maximum p_T particle on that side. (The maximum p_T particle is not included in the plot.)

Five plots corresponding to 1 GeV/c intervals in p_T of the charged particle are shown. The data is for trigger $p_T > 7$ GeV/c.

Fig. 5 : Away-side charged particle correlation functions.

a) $\bar{f}$ as defined in the text plotted as a function of the charged particle p_T for the three sets of trigger $p_{T\,t}$ and the zero threshold sample.

b) f_{max} plotted as $\bar{f}$ above.

c) $\bar{F}$ plotted as a function of trigger $p_{T\,t}$ after integrating over charged particle $p_T > 0.3$ GeV/c.

d) F_{max} plotted as $\bar{F}$ in (c).

Fig. 6 : A diagram showing the definition of variables used to relate particles to the trigger.

Fig. 7 : a) and b) $\langle |p_{out}| \rangle$ of away-side charged particles relative to the trigger for the three sets of trigger $p_{T\,t}$.

Fig. 8 : dn/dx_E distribution of away-side charged particles relative to the neutral trigger for the three sets as above.

Fig. 9 : $dN/d(\Sigma x_E)$ distribution for away-side charged particles in $|\phi-\pi| < \pi/3$ relative to the neutral trigger for the three sets of trigger $p_{T\,t}$.

Fig. 10 : dn/dp_T distribution of same-side charged particles in $|\phi| < \pi/3$ for the three sets of trigger p_T. The zero threshold spectrum is also shown.

Fig. 11 : $\langle \Sigma x_E \rangle$ for same-side charged particles in $|\phi| < \pi/3$ as a function of trigger p_T.

Fig. 12 : dn/dp_T for charged particles in two azimuthal regions between the correlated ϕ peaks ($\pi/3 < |\phi| < 2\pi/3$). The zero threshold dn/dp_T spectrum is also shown.

Fig. 13 : Diagram showing the definition of variables used in the vector sum analysis.

Fig. 14 : a) $\langle |p_{out\,\phi}| \rangle$ of particles relative to the away-side vector sum. The two Monte Carlo predictions described in the text are shown.

b) $\langle |p_{out\,\theta}| \rangle$ particles relative to the away-side vector sum. The Monte Carlo prediction described in the text is shown.

The track p_T distributions used in the Monte Carlo did not extend beyond 5 GeV/c.

a)

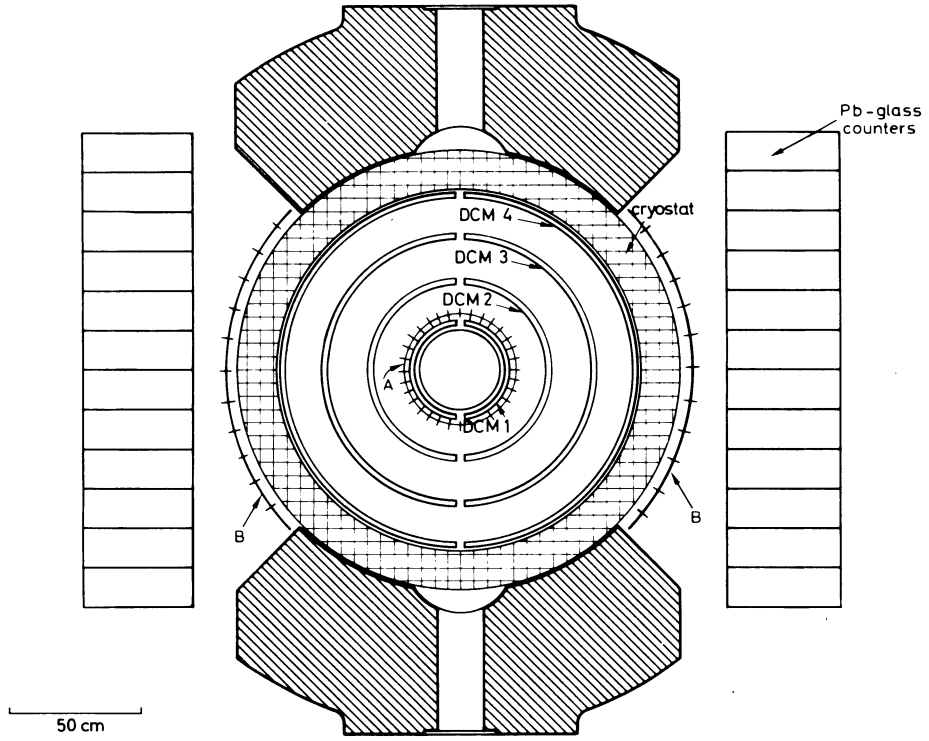
Pb-glass
counters
cryostat
DCM 4
DCM 3
DCM 2
DCM 1
A
B
B
50 cm

b)

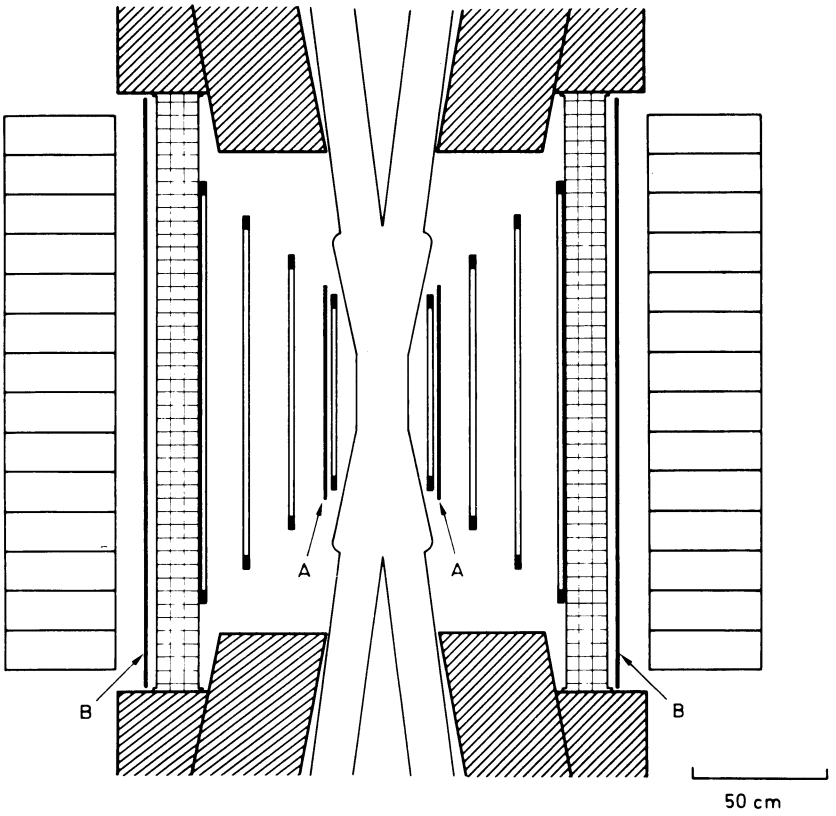
A
A
B
B
50 cm

Fig. 1

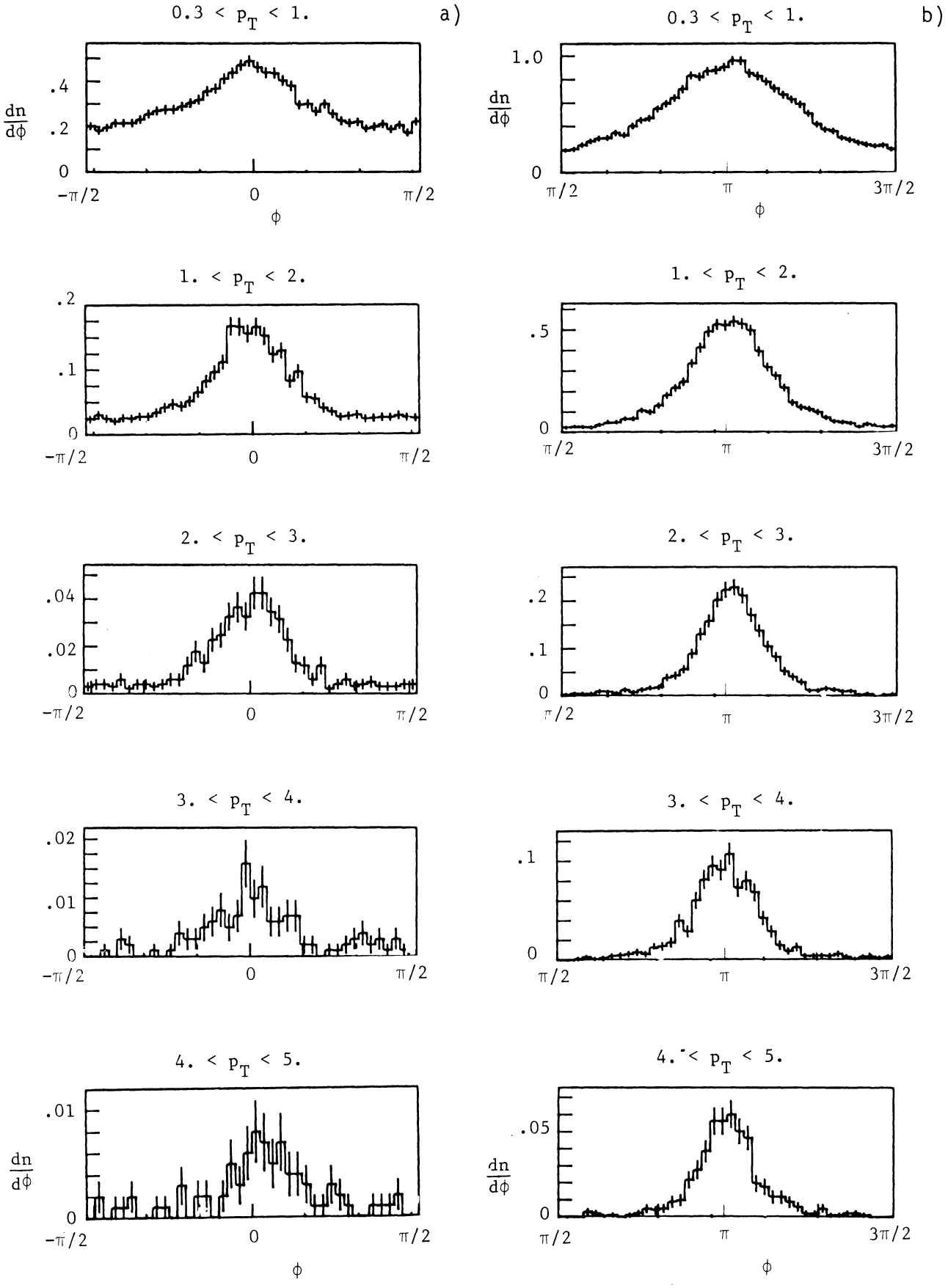

Fig. 2

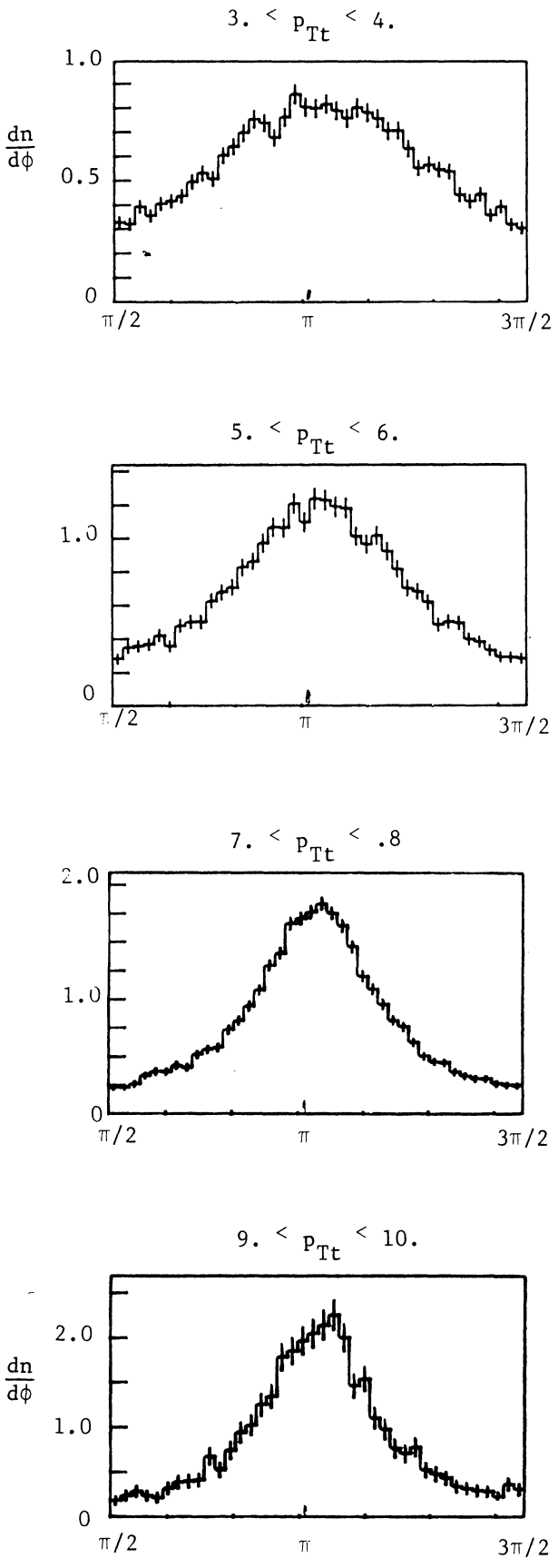
3. < p_{Tt} < 4.
1.0
0.5
0
$\frac{dn}{d\phi}$
π/2
π
3π/2
5. < p_{Tt} < 6.
1.0
0
π/2
π
3π/2
7. < p_{Tt} < .8
2.0
1.0
0
π/2
π
3π/2
9. < p_{Tt} < 10.
2.0
1.0
0
$\frac{dn}{d\phi}$
π/2
π
3π/2

Fig. 3

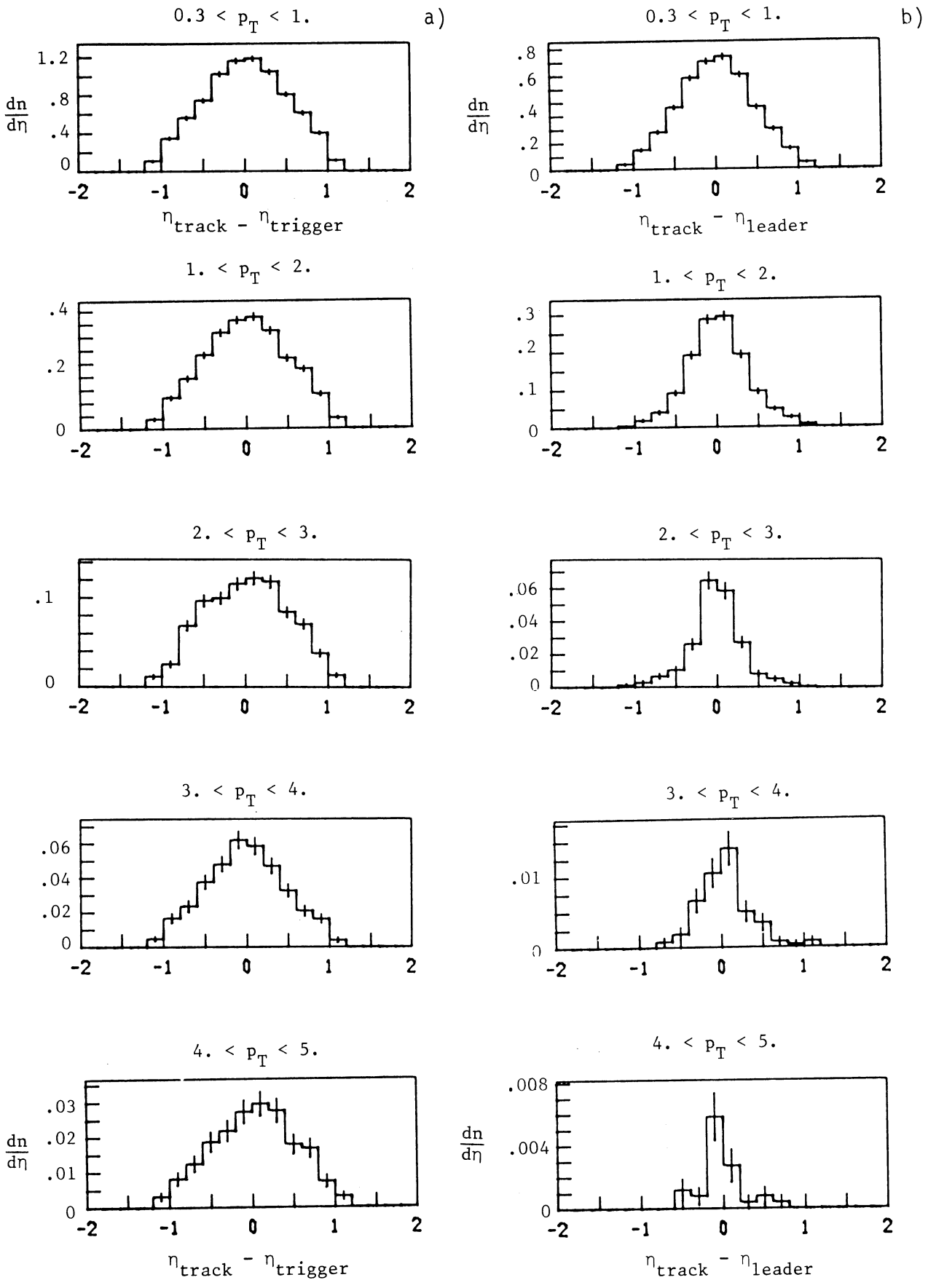
a)
b)
0.3 < p_T < 1.
1. < p_T < 2.
2. < p_T < 3.
3. < p_T < 4.
4. < p_T < 5.
$\frac{dn}{d\eta}$
$\eta_{track} - \eta_{trigger}$
$\eta_{track} - \eta_{leader}$

Fig. 4

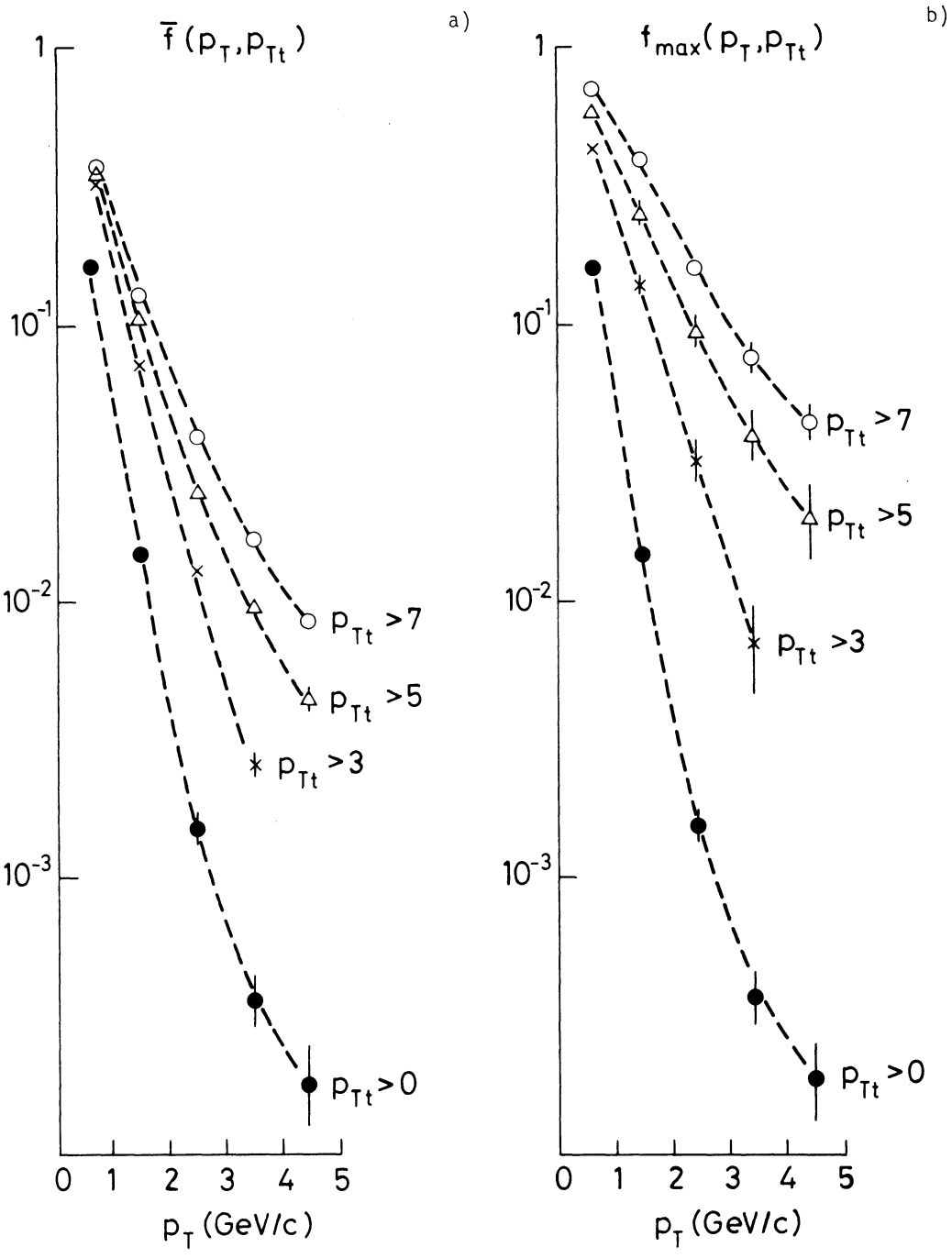
a)
$\bar{f}(p_T, p_{Tt})$
1
10^{-1}
10^{-2}
10^{-3}
$p_{Tt}>7$
$p_{Tt}>5$
$p_{Tt}>3$
$p_{Tt}>0$
0 1 2 3 4 5
p_T (GeV/c)
b)
$f_{max}(p_T, p_{Tt})$
1
10^{-1}
10^{-2}
10^{-3}
$p_{Tt}>7$
$p_{Tt}>5$
$p_{Tt}>3$
$p_{Tt}>0$
0 1 2 3 4 5
p_T (GeV/c)

Fig. 5 (a) (b)

c)

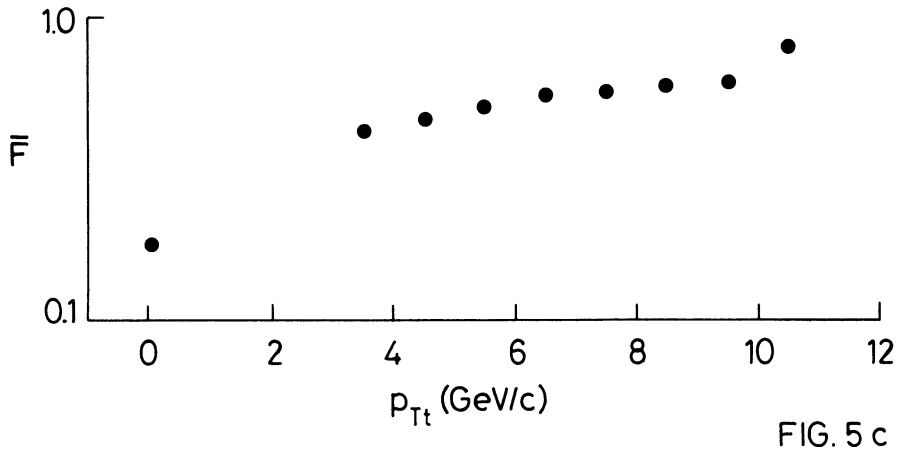

FIG. 5 c

d)

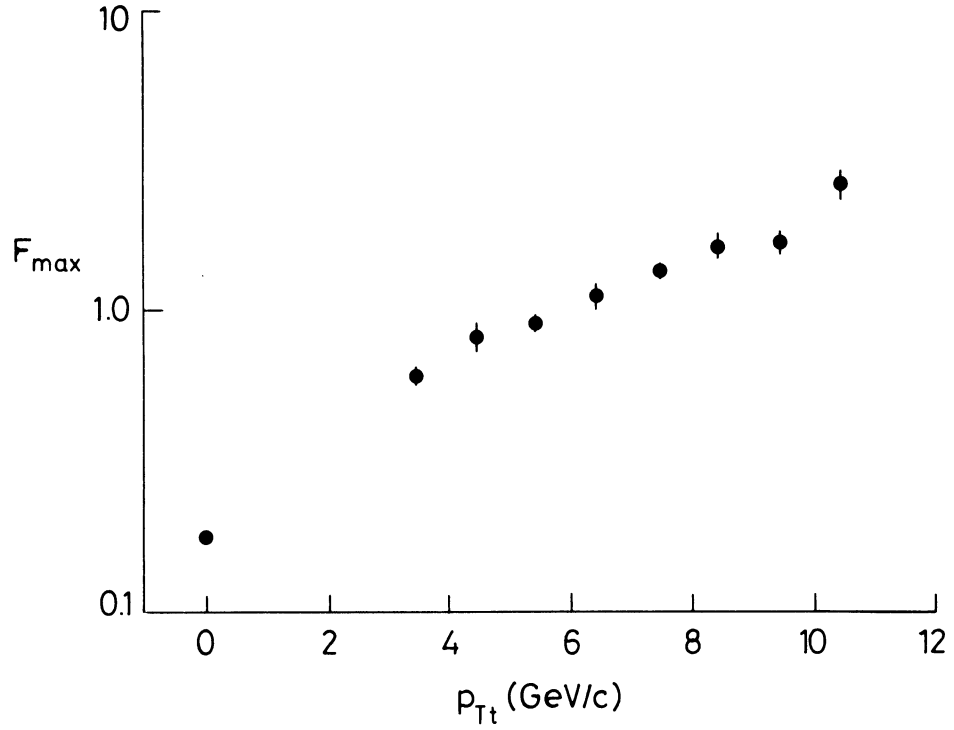

Fig. 5 (c) (d)

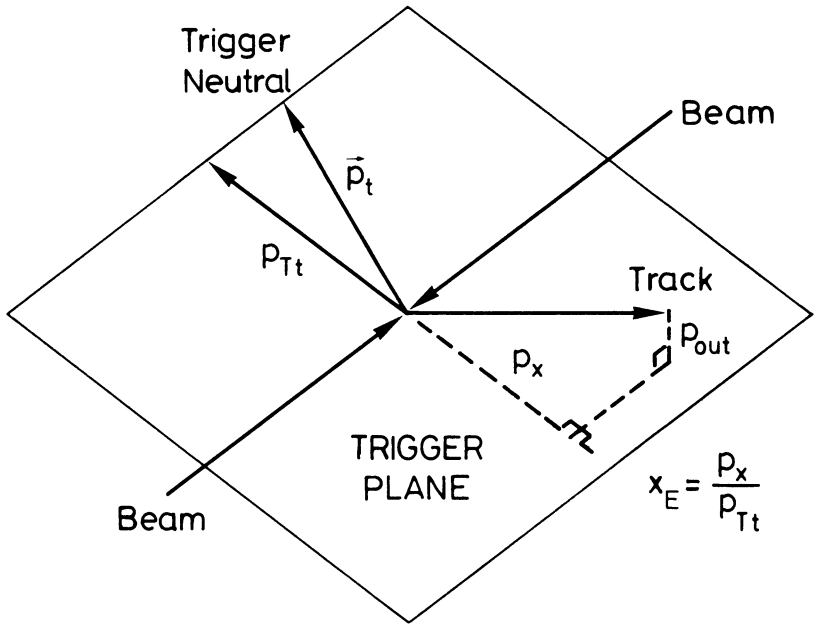
Trigger
Neutral
Beam
$\vec{p}_t$
p_{Tt}
Track
p_{out}
p_x
TRIGGER
PLANE
Beam
$x_E = \frac{p_x}{p_{Tt}}$

Fig. 6

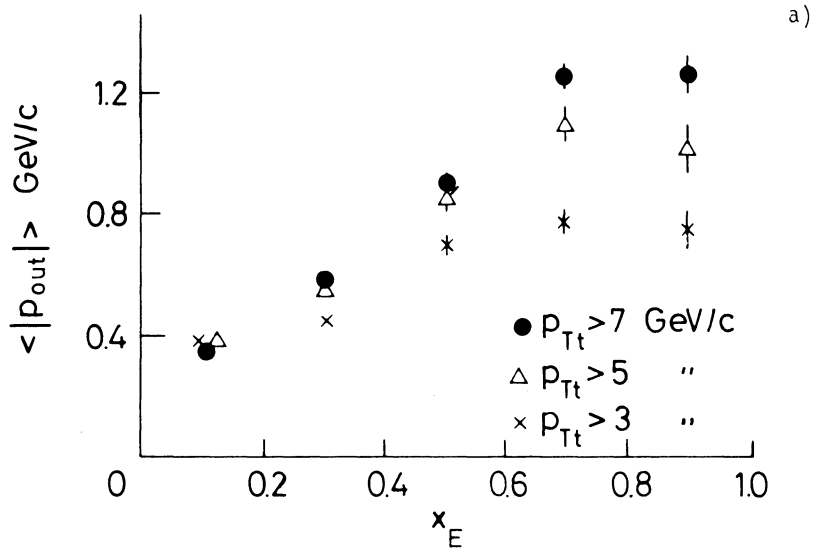
a)
1.2
0.8
0.4
0
0.2
0.4
0.6
0.8
1.0
x_E
$\langle |p_{out}| \rangle$ GeV/c
p_{Tt}>7 GeV/c
p_{Tt}>5 "
p_{Tt}>3 "

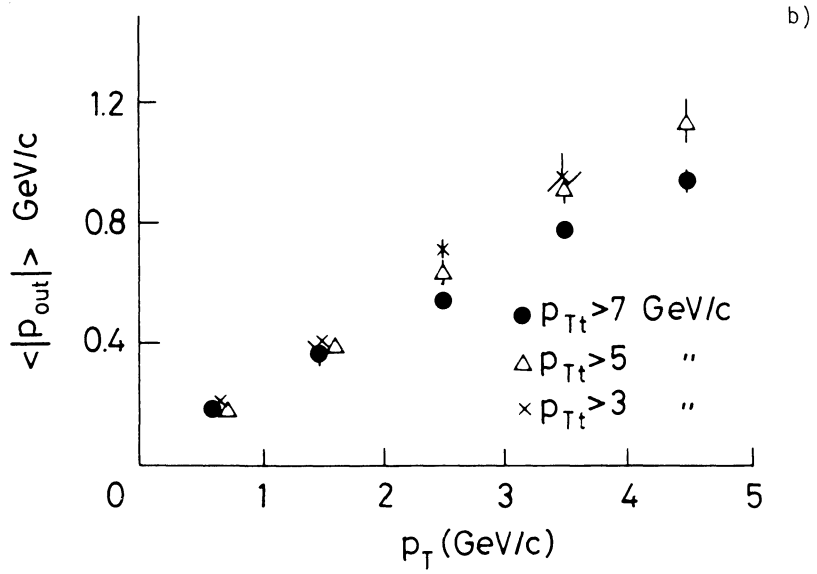
b)
1.2
0.8
0.4
0
1
2
3
4
5
p_T (GeV/c)
$\langle |p_{out}| \rangle$ GeV/c
p_{Tt}>7 GeV/c
p_{Tt}>5 "
p_{Tt}>3 "

Fig. 7

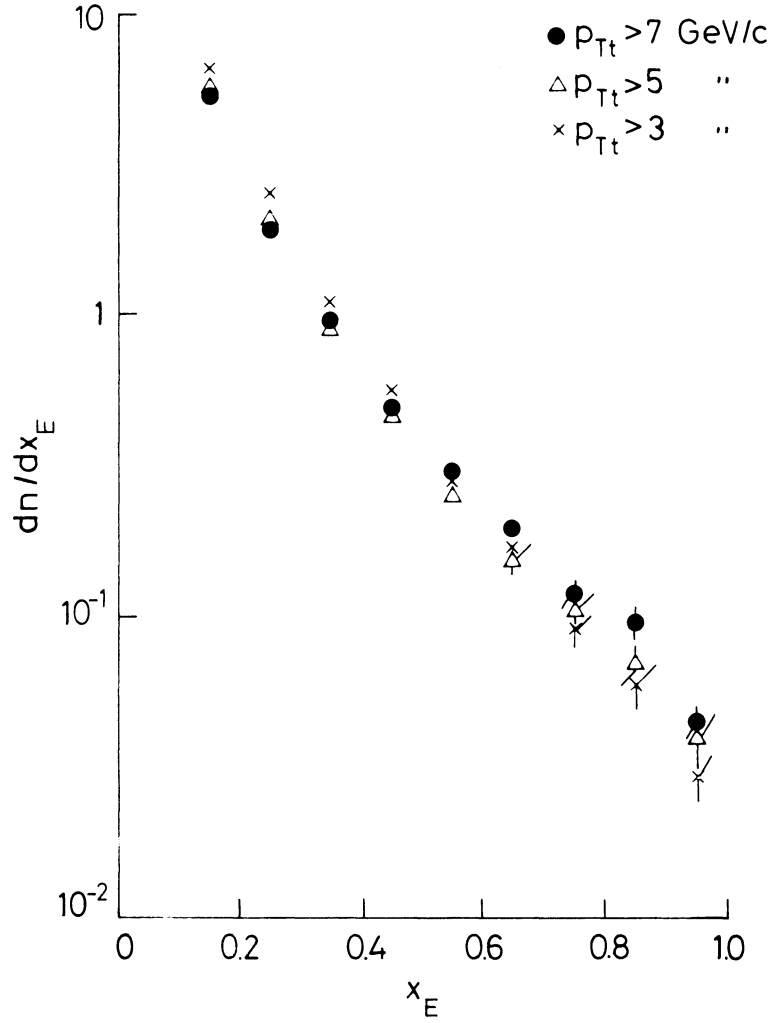

Fig. 8

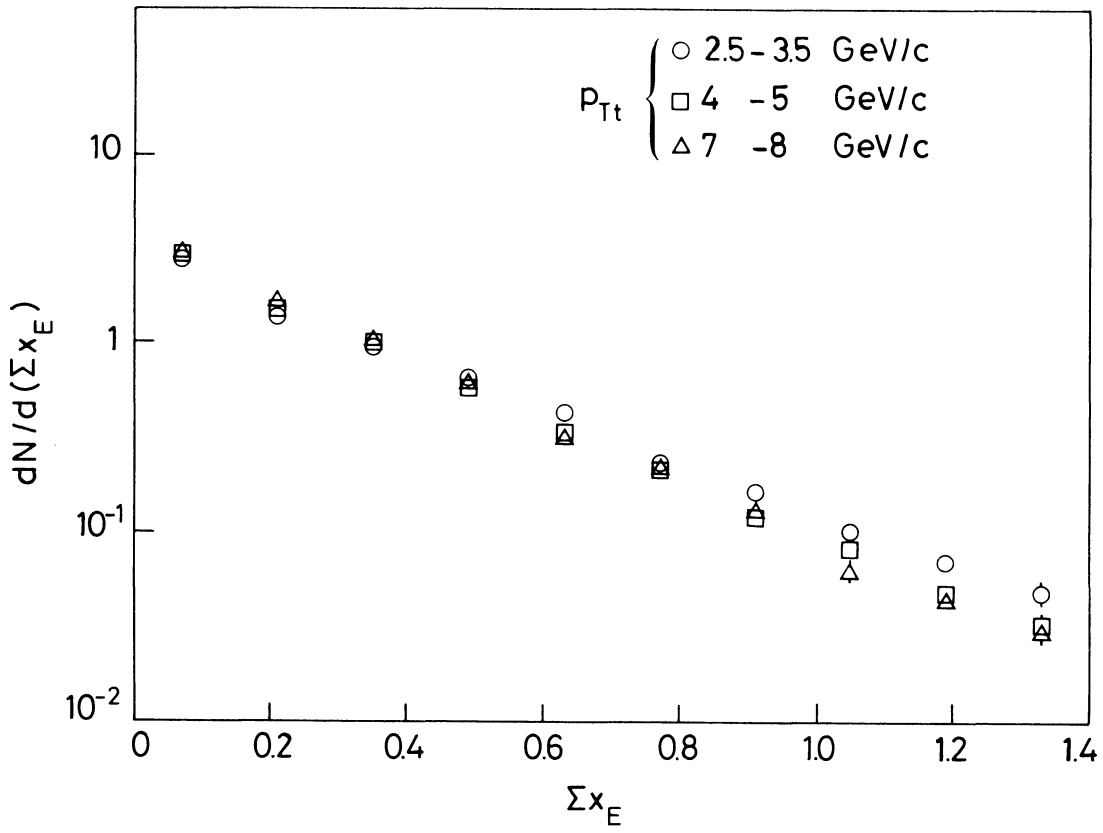
P_{Tt}
○ 2.5-3.5 GeV/c
□ 4 -5 GeV/c
△ 7 -8 GeV/c
$dN/d(\Sigma x_E)$
Σx_E
10
1
10^{-1}
10^{-2}
0
0.2
0.4
0.6
0.8
1.0
1.2
1.4

Fig. 9

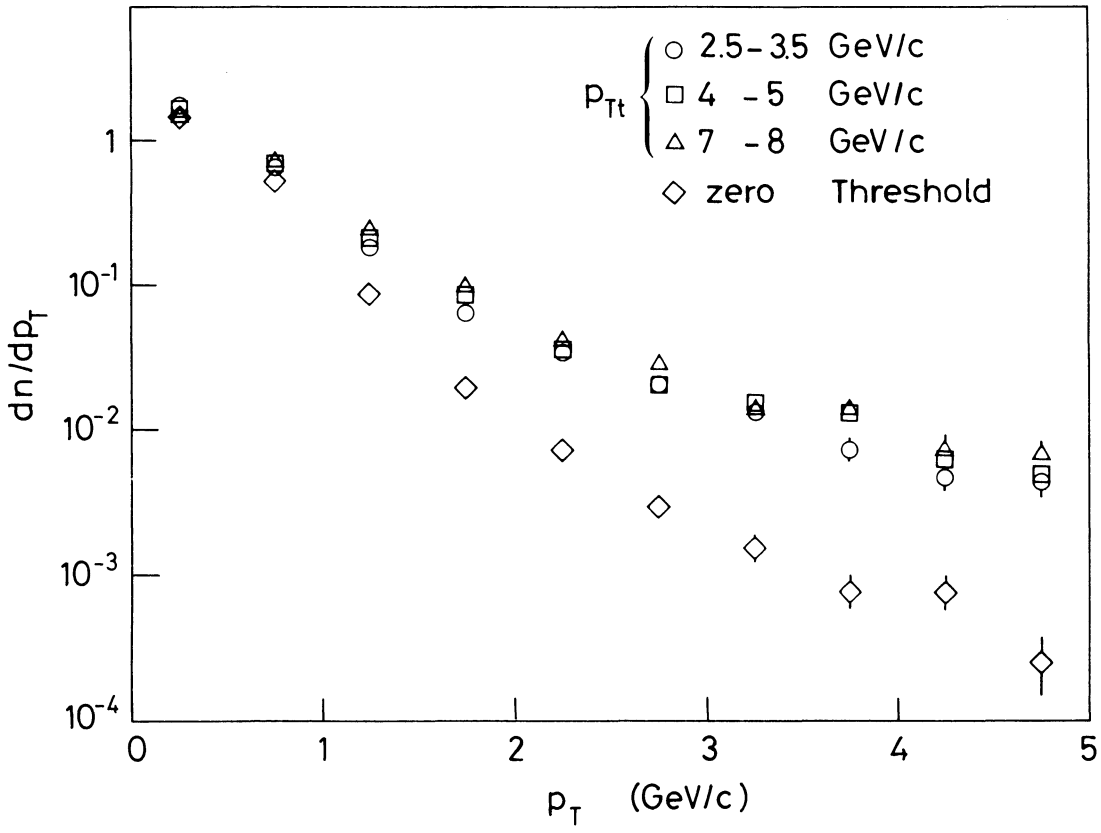
P_{Tt}
○ 2.5-3.5 GeV/c
□ 4 -5 GeV/c
△ 7 -8 GeV/c
◇ zero Threshold
dn/dp_T
p_T (GeV/c)
1
10^{-1}
10^{-2}
10^{-3}
10^{-4}
0
1
2
3
4
5

Fig. 10

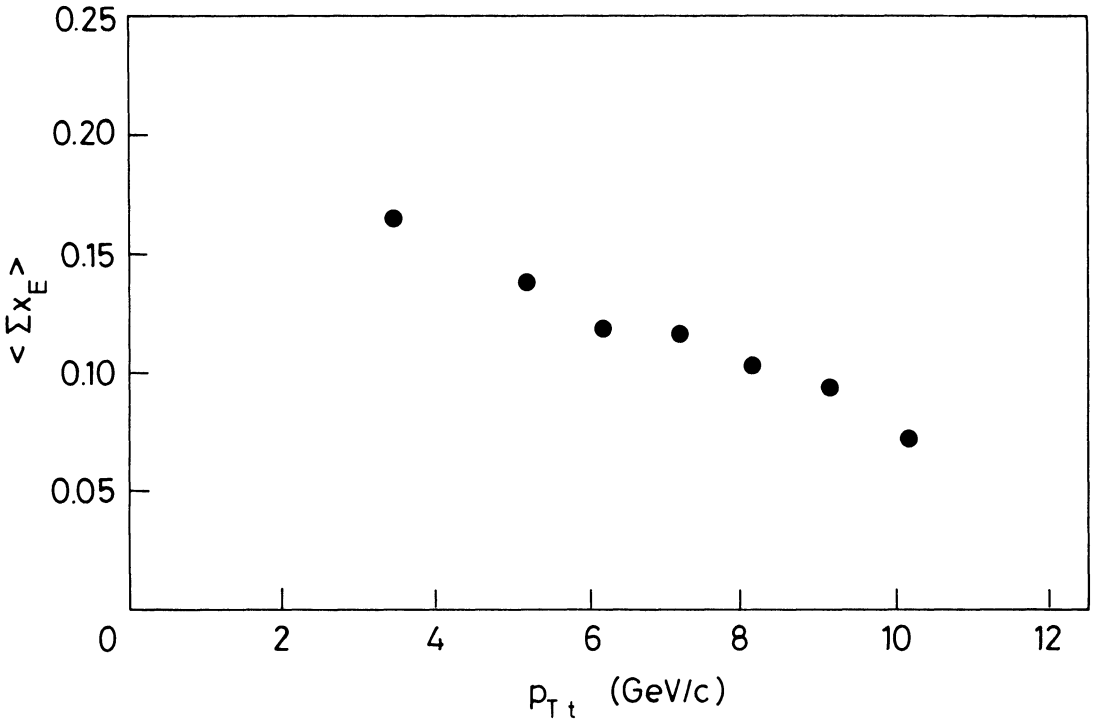
0.25
0.20
0.15
0.10
0.05
$\langle \Sigma x_E \rangle$
0
2
4
6
8
10
12
$p_{T\,t}$ (GeV/c)

Fig. 11

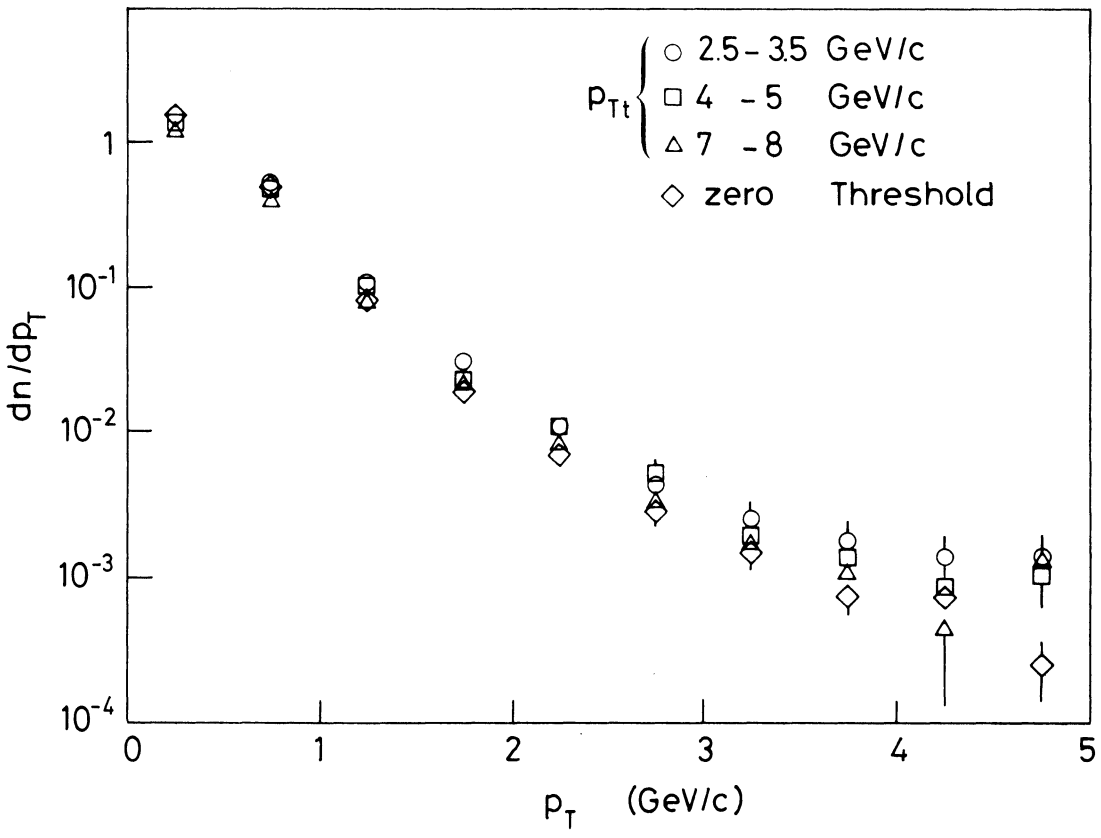
p_{Tt}
○ 2.5 - 3.5 GeV/c
□ 4 - 5 GeV/c
△ 7 - 8 GeV/c
◇ zero Threshold
1
10^{-1}
10^{-2}
10^{-3}
10^{-4}
dn/dp_T
0
1
2
3
4
5
p_T (GeV/c)

Fig. 12

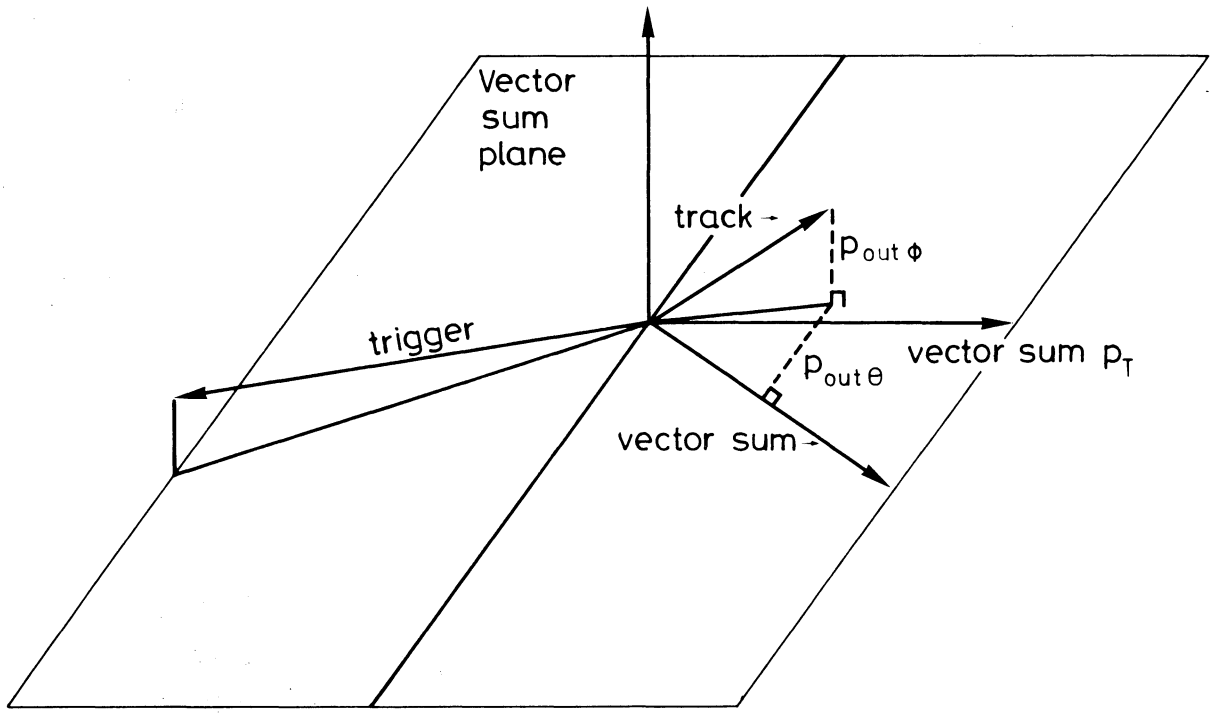
Vector
sum
plane
track
$p_{out\,\phi}$
trigger
vector sum p_T
$p_{out\,\theta}$
vector sum

Fig. 13

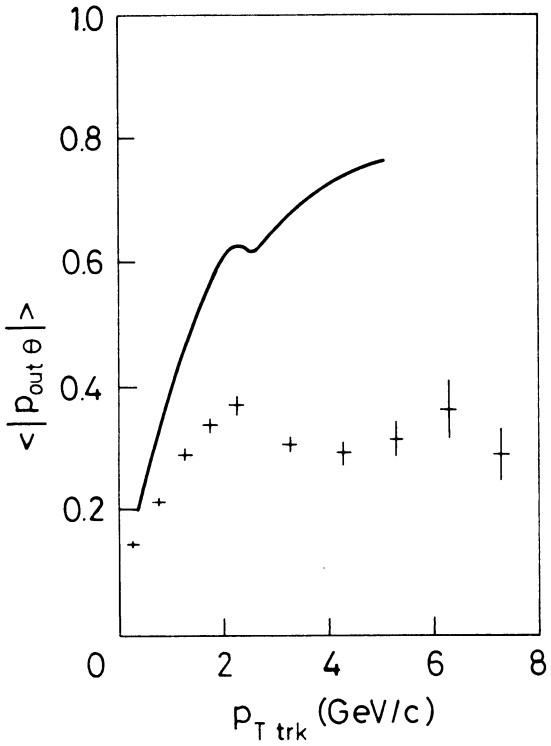
1.0
0.8
0.6
0.4
0.2
0
2
4
6
8
$\langle |p_{out\,\theta}| \rangle$
$p_{T\,trk}$ (GeV/c)

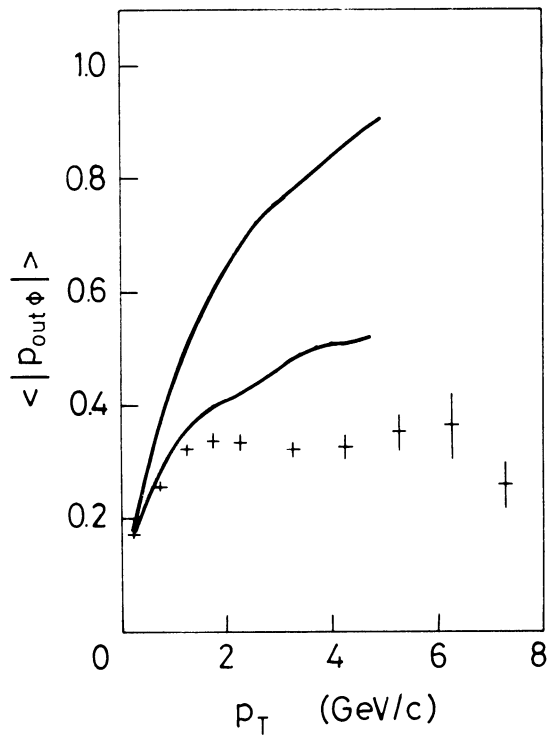
1.0
0.8
0.6
0.4
0.2
0
2
4
6
8
$\langle |p_{out\,\phi}| \rangle$
p_T (GeV/c)

Fig. 14